Bioorganic & Medicinal Chemistry 17 (2009) 5259–5274

Contents lists available at ScienceDirect

Bioorganic & Medicinal Chemistry

journal homepage: www.elsevier.com/locate/bmc

Combining selectivity and affinity predictions using an integrated Support Vector Machine (SVM) approach: An alternative tool to discriminate between the human adenosine A_{2A} and A_3 receptor pyrazolo-triazolo-pyrimidine antagonists binding sites

Lisa Michielan [a], Chiara Bolcato [b], Stephanie Federico [b], Barbara Cacciari [c], Magdalena Bacilieri [a], Karl-Norbert Klotz [d], Sonja Kachler [d], Giorgia Pastorin [e], Riccardo Cardin [f], Alessandro Sperduti [f], Giampiero Spalluto [b,*], Stefano Moro [a,*]

[a] Molecular Modeling Section (MMS), Dipartimento di Scienze Farmaceutiche, Università di Padova, via Marzolo 5, I-35131 Padova, Italy
[b] Dipartimento di Scienze Farmaceutiche, Università di Trieste, Piazzale Europa 1, I-34127, Trieste, Italy
[c] Dipartimento di Scienze Farmaceutiche, Università degli Studi di Ferrara, Via Fossato di Mortara 17-19, I-44100 Ferrara, Italy
[d] Institut für Pharmakologie, Universität of Würzburg, D-97078 Würzburg, Germany
[e] Department of Pharmacy, National University of Singapore, Block S4, 18 Science Drive 4, Singapore
[f] Dipartimento di Matematica Pura ed Applicata, Universitá di Padova, Via Trieste 63, I-35121 Padova, Italy

ARTICLE INFO

Article history:
Received 19 February 2009
Revised 8 May 2009
Accepted 14 May 2009
Available online 21 May 2009

Keywords:
Adenosine receptors
G protein-coupled receptor
Selectivity profile
Support Vector Machine
QSAR

ABSTRACT

G Protein-coupled receptors (GPCRs) selectivity is an important aspect of drug discovery process, and distinguishing between related receptor subtypes is often the key to therapeutic success. Nowadays, very few valuable computational tools are available for the prediction of receptor subtypes selectivity.

In the present study, we present an alternative application of the Support Vector Machine (SVM) and Support Vector Regression (SVR) methodologies to simultaneously describe both A_{2A}R versus A_3R subtypes selectivity profile and the corresponding receptor binding affinities. We have implemented an integrated application of SVM–SVR approach, based on the use of our recently reported autocorrelated molecular descriptors encoding for the Molecular Electrostatic Potential (*auto*MEP), to simultaneously discriminate A_{2A}R versus A_3R antagonists and to predict their binding affinity to the corresponding receptor subtype of a large dataset of known pyrazolo-triazolo-pyrimidine analogs. To validate our approach, we have synthetized 51 new pyrazolo-triazolo-pyrimidine derivatives anticipating both A_{2A}R/A_3R subtypes selectivity and receptor binding affinity profiles.

1. Introduction

More than 50% of prescription drugs act on G protein-coupled receptors (GPCRs). However, some have efficacy problems and limiting side-effects because the compounds do not differentiate between receptor subtypes. There is thus considerable interest in attaining therapeutic selectivity by identifying the single receptor subtype that affects a particular physiology. The goal is to be able to design drugs without, or at least with less, side-effects, while retaining the desired function. Nowadays, very few valuable computational tools are available for the prediction of receptor subtypes selectivity. Conversely, different in silico approaches are accessible for the prediction of the distinct receptor–ligand affinity. In particular, the generation of a quantitative structure–activity relationship (QSAR) is probably one of the most robust and validated approach to mathematically achieve the correlation between molecular properties and the corresponding receptor–ligand affinity.[1,2]

In the last few years, we have intensively explored the possibility to discover new potent and selective adenosine receptors (ARs) antagonists. Briefly, the adenosine receptor (AR) family belongs to GPCR family A, which includes four different subtypes, referred to as A_1, A_{2A}, A_{2B} and A_3, which are widely but differentially distributed throughout the body.[3,4] Interestingly, both A_{2A}R and A_3R receptor selective ligands are becoming increasingly attractive drugs due to the potential role of this receptor in several physiopathological processes.[5–9] In particular, A_{2A}R antagonists seem to

Abbreviations: AR, adenosine receptor; h, human; TM, transmembrane; EL2, second extracellular loop; GPCR, G protein-coupled receptor; SVM, Support Vector Machine; SVR, Support Vector Regression; *auto*MEP, autocorrelated Molecular Electrostatic Potential; QSAR, quantitative structure–activity relationship.

* Corresponding authors. Tel.: +39 049 8275704; fax: +39 049 8275366 (S.M.).
E-mail address: stefano.moro@unipd.it (S. Moro).

0968-0896/$ - see front matter © 2009 Published by Elsevier Ltd.
doi:10.1016/j.bmc.2009.05.038

play a role in the reduction of neuronal damage in Parkinson's or Huntington's diseases, while A_3R antagonists have a potential application in the tumor growth inhibition and in the treatment of glaucoma.[4,7,10] Consequently, several receptor-based and ligand-based drug design approaches have been carried out with the aim to improve potency and selectivity of different molecular scaffolds. Among them, the pyrazolo-triazolo-pyrimidine scaffold has been used as one of the most versatile scaffold in designing novelty among adenosine receptors antagonists.[11] In particular, proper substitutions at the N^5 and N^8 positions have driven the antagonist selectivity to the human A_3R subtype.[11] On the other hand, it has been also demonstrated that the substitution at the position N^7 shifts the selectivity profile to the human $A_{2A}R$ subtype.[12] Nevertheless, besides this very empirical rule derived only by experimental evidences, it is very difficult to anticipate the correct pharmacological receptor profiles of novel pyrazolo-triazolo-pyrimidine derivatives and, at the same time, inferring in their receptor–ligand affinities.

In the present study, we present an alternative application of the Support Vector Machine (SVM) and Support Vector Regression (SVR) methodologies to simultaneously describe both $A_{2A}R$ versus A_3R subtypes selectivity profile and the corresponding receptor binding affinities. SVM represents a group of supervised learning techniques, firstly applied in pattern recognition, but now very utilized to solve both classification and regression problems.[13,14] In the last years, several classification problems have been solved, in fact, using SVM approach, such as, for example, the discrimination between active and non-active compounds.[15–18] Moreover, Support Vector Regression (SVR) has been widely applied as a non-linear methodology to derive quantitative structure–activity relationships for the prediction of different chemical and biological properties.[19–23] Moving from these examples, we have implemented an integrated application of SVM–SVR approach, based on the use of our recently reported autocorrelated molecular descriptors encoding for the Molecular Electrostatic Potential (*auto*MEP), to simultaneously discriminate $A_{2A}R$ versus A_3R antagonists and to predict their binding affinity to the corresponding receptor subtype of a large dataset of known pyrazolo-triazolo-pyrimidine analogs.[24–28] To validate our approach, we have synthetized 51 new pyrazolo-triazolo-pyrimidine derivatives anticipating both $A_{2A}R/A_3R$ subtypes selectivity and receptor binding affinity profiles. The statistical quality of both training and validation models are very encouraging.

2. Materials and methods

2.1. Computational methodologies

All modeling studies were carried out on a linux cluster running under openMosix architecture.[29] Molecular structure building and autocorrelation MEP descriptors have been carried out using ADRIANACODE software (version 2.0).[30] Support Vector Machine classification and Support Vector Regression have been performed using SVM^{light} software.[31]

2.2. Molecular structure building

3D Models of the pyrazolo-triazolo-pyrimidine analogs in the training set and some analogs in the test set were obtained using the 3D structure generator Corina, which is an integral part of ADRIANACODE, setting parameters to standard values.[30] Conformer selection is one of the most crucial steps in every 3D-QSAR approach. Unfortunately, the information about the possible binding mode of all A_{2A} and A_3 receptor antagonists are limited and consequently we have decided to select the energetically most stable conformers produced by the software conformational analysis.

2.3. Training set 1

SVM classification (SVMclass) model: A collection of 104 selective N^7- and N^8-substituted pyrazolo-triazolo-pyrimidine analogues (**1**–**104**) has been selected as training set in the SVM*class* model.[11,12,32–36] See Supplementary data for details.

2.4. Training set 2

SVR regression (SVR) model: A collection of 104 N^8-substituted pyrazolo-triazolo-pyrimidine derivatives (**1–71**, **105–137**), A_{2A} and A_3 selective and non-selective compounds, has been used as training set of both human $A_{2A}R$ and A_3R non-linear SVR models.[11,12,32,33,37] See Supplementary data for details.

2.5. Test set

A test set of 51 N^8-substituted pyrazolo-triazolo-pyrimidine analogues (**138**–**188**) has been selected to validate both SVM*class* and SVR models. See Table 1.

2.6. Molecular Electrostatic Potential (MEP) calculation

Autocorrelation MEP vectors have been introduced by Gasteiger and collaborators as molecular descriptors computed on the molecular surface.[38] In the present work, MEPs derive from a classical point charge model: the electrostatic potential for each molecule is obtained by moving a unit positive point charge across the molecular surface, and it is calculated at various points *j* on this surface by the following equation:

$$V_j = \sum_i^{\text{atoms}} \frac{q_i}{r_{ji}}$$

where q_i represents the partial charge of each atom *i* and r_{ji} is the distance between points *j* and atom *i*. Starting from the 3D model of a molecule and its partial atomic charges, the electrostatic potential is calculated for points on the molecular surface. Partial atomic charges were calculated by the PEOE (*P*artial *E*qualization of *O*rbital *E*lectronegativity) method and its extension to conjugated systems implemented in ADRIANACODE.[30,39,40] Connolly's solvent accessible surface with a solvent radius of 2.0 Å has been used to project the corresponding MEP. Once the autocorrelation function has been applied, the autocorrelation vector is derived. Connolly's solvent accessible surfaces and the corresponding MEPs have been calculated by ADRIANACODE.[30,39,40]

2.7. Autocorrelation MEP (autoMEP) vectors

The idea of using autocorrelation for the transformation of the constitution of a molecule into a fixed length representation was introduced by Moreau and Broto.[41,42] They considered that a certain property *p* of an atom *i* can be correlated with the same property *p* of atom *j* and the products of *p* values can be summed over all atom pairs having a certain topological distance *d*. Each component of the autocorrelation vector is consequently calculated as follows

$$A(d) = \sum_{ij} p_i p_j$$

where *A* is the autocorrelation coefficient referring to atom pairs *i,j* at the *i,j* topological distance *d* and p_i is the atomic property.[41,42]

Table 1
Biological profile at the hA_1 and hA_{2B} receptor subtypes of synthesized (**138**–**188**) compounds

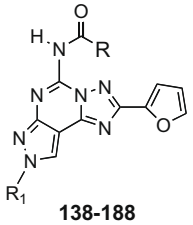

138-188

Mol	R	R_1	hA_1 (K_i nM)[a]	hA_{2A} K_i (nM)	hA_{2B} IC_{50} (nM)[b]	hA_3 (K_i nM)
138	CH_2-α-Naphthyl	$CH_2CH_2CH_2Ph$	710 (425–1180)	305	>100,000	343
139	$CHPh_2$	CH_3	139 (82.7–235)	216	363 (318–414)	0.25
140	CH_2-Ph-Ph	CH_3	1460 (1,010–2.100)	193	>10,000	11.2
141	$CHPh_2$	$CH_2CH_2CH(CH_3)_2$	441 (281–692)	159	>10,000	5.86
142	CH_2-Ph-Ph	$CH_2CH_2CH(CH_3)_2$	84.3 (80.7–88)	9.18	8960 (5880–12,700)	268
143	$CHPh_2$	CH_2CH_2Ph	115 (90.7–147)	53.1	5840 (2920–11,600)	6.49
144	CH_2-Ph-Ph	CH_2CH_2Ph	84.3 (67.4–105)	46.9	11,100 (5110–24,100)	125
145	$CHPh_2$	$CH_2CH_2CH_2CH_3$	129 (92.6–180)	114	780 (650–936)	1.20
146	CH_2-Ph-Ph	$CH_2CH_2CH_2CH_3$	381 (276–527)	39.6	8630 (4810–15,500)	189
147	CH_2-3-Cl-Ph	CH_3	410 (352–478)	30.5	8960 (5580–12,700)	1.94
148	$CHPh_2$	$CH_2CH_2CH_3$	80.2 (49.7–129)	46.5	491 (327–736)	0.93
149	CH_2-Ph-Ph	$CH_2CH_2CH_3$	622 (424–912)	52.5	>10,000	65.4
150	CH_2-4-Cl-Ph	CH_3	1850 (1250–2740)	156	>50,000	12.7
151	CH_2-Ph-Ph	CH_2CH_3	557 (432–717)	70.9	>50,000	14.2
152	CH_2-4-OCH_3-Ph	CH_3	133 (103–170)	62.5	>10,000	0.95
153	CH_2-β-Naphthyl	$CH_2CH_2CH(CH_3)_2$	140 (75.9–258)	15.7	>10,000	409
154	CH_2-β-Naphthyl	CH_2CH_2Ph	57.5 (38.7–85.5)	42.1	>50,000	180
155	CH_2-2-Thienyl	CH_2CH_2Ph	18.5 (16.21.4)	8.8	>10,000	330
156	CH_2-3-Thienyl	CH_2CH_2Ph	22.8 (16.9–30.6)	12.9	>10,000	726
157	CH_2-α-Naphthyl	CH_2CH_3	596 (428–829)	74.6	>50,000	3.05
158	CH_2-β-Naphthyl	CH_2CH_3	185 (147–233)	18.4	10,370 (7870–13,700)	36.3
159	CH_2-3-Thienyl	CH_2CH_3	154 (68.5–345)	23	9370 (8830–9950)	765
160	CH_2-2-Thienyl	CH_2CH_3	148 (116–189)	15.9	15,000 (13,500–16,600)	196
161	CH_2-2-Thienyl	CH_3	444 (390–505)	56	>10,000	5.26
162	CH_2-3-Thienyl	CH_3	461 (380–560)	31.3	13,700 (10,100–18,500)	1.25
163	CH_2-β-Naphthyl	CH_3	190 (155–232)	77.5	>10,000	14.5
164	CH_2-α-Naphthyl	CH_3	872 (722–1050)	80.5	>10,000	3.47
165	CH_2-α-Naphthyl	$CH_2CH_2CH_3$	388 (256–587)	38.7	12,400 (8680–17,800)	17.3
166	CH_2-β-Naphthyl	$CH_2CH_2CH_3$	160 (109–233)	7.99	5370 (3490–8120)	95.9
167	CH_2-α-Naphthyl	$CH_2CH_2CH_2CH_3$	170 (129–255)	11.7	7370 (5000–10,900)	100
168	CH_2-4-CF_3-Ph	CH_3	768 (594–994)	75.9	>10,000	1.22
169	CH_2-2-Thienyl	$CH_2CH_2CH_2CH_3$	70.1 (60.6–81.1)	4.15	1810 (1170–2800)	99.8
170	CH_2-3-Thienyl	$CH_2CH_2CH_2CH_3$	25.5 (8.33–78.2)	3.13	906 (804–1020)	189
171	CH_2-O-Ph-4-Cl	CH_3	963 (843–1100)	39.3	>10,000	223
172	CH_2-3-Cl-Ph	$CH_2CH_2CH(CH_3)_2$	13.7 (3.73–50.4)	1.86	1390 (990–1940)	273
173	CH_2-4-Cl-Ph	$CH_2CH_2CH(CH_3)_2$	22.6 (18.1–28.2)	2.75	1220 (1020–1470)	56.5
174	CH_2-3-Cl-Ph	CH_2CH_2Ph	13.2 (11.5–15.2)	5.75	9100 (6600–12,600)	273
175	CH_2-4-CF_3-Ph	$CH_2CH_2CH(CH_3)_2$	48.2 (31.4–74.2)	5.43	5480 (4570–7470)	266
176	CH_2-4-F-Ph	$CH_2CH_2CH(CH_3)_2$	51.8 (30.5–88)	3.69	5060 (3440–7450)	116
177	CH_2-4-F-Ph	CH_3	741 (615–892)	54.1	13,000 (9520–17,700)	0.97
178	CH_2-2,6-Cl_2-Ph	$CH_2CH_2CH(CH_3)_2$	121 (86.1–169)	18.7	1440 (618–3350)	207
179	CH_2-2,6-Cl_2-Ph	CH_3	908 (874–944)	45.2	6450 (3930–10,600)	44.4
180	CH_2-4-F-Ph	$CH_2CH_2CH_2Ph$	726 (563–935)	211	>50,000	58.5
181	CH-Ph_2	$CH_2CH_2CH_2Ph$	307 (276–340)	326	>10,000	12.6
182	CH_2-β-Naphthyl	$CH_2CH_2CH_2Ph$	241 (218–267)	73.6	>50,000	717
183	CH_2Ph	$CH_2CH_2CH_2Ph$	128 (113–144)	43.9	>3000	5.49
184	CH_2-3-Cl-Ph	$CH_2CH_2CH_2Ph$	605 (578–633)	182	50,000	110
185	CH_2-4-Cl-Ph	$CH_2CH_2CH_2Ph$	256 (190–346)	89.9	>10,000	30.5
186	CH_2-O-Ph-4-Cl	$CH_2CH_2CH_2Ph$	71.1 (48.3–105)	27.2	>10,000	400
187	CH_2-2,6-Cl_2-Ph	$CH_2CH_2CH_2Ph$	786 (607–1000)	186	>10,000	601
188	CH_2-Ph-Ph	$CH_2CH_2CH_2Ph$	1,170 (1040–1300)	256	>100,000	410

[a] Displacement of specific [^{3}H]-CCPA binding at human A_1 receptors expressed in CHO cells (n = 3–6).
[b] K_i values of the inhibition of NECA-stimulated adenylyl cyclase activity in CHO cells expressing hA_{2B} receptors. Data are expressed as geometric means, with 95% confidence limits.

Ligands and proteins interact through molecular surfaces and, therefore, representations of molecular surfaces have to be sought in the endeavor to understand biological activity. Again, we are under the restriction of having to represent molecular surfaces of different size, and consequently Gasteiger and collaborators employed the autocorrelation concept to achieve this

goal.[40,43,44] Starting form the topological autocorrelation examples of Moreau and Broto, firstly they generated a set of randomly distributed points on the molecular surface, then, all distances between the surface points were calculated and sorted into preset intervals $d_{\text{lower}} - d_{\text{upper}}$. The autocorrelation coefficients are then computed:

$$A(d_{\text{lower}}, d_{\text{upper}}) = 1/L \sum p_i p_j (d_{\text{lower}} < d_{ij} < d_{\text{upper}}),$$

where the *i*,*j* distance *d* belongs to the $d_{\text{lower}} - d_{\text{upper}}$ interval and *L* is the total number of distances in the same interval. The application of this concept made possible to compare different molecular properties, since this 3D descriptor represents a compressed expression of the distribution of the property *p* on the molecular surface.

For the calculation of the autocorrelation coefficient we have applied the default values for parameters computation, since no improving in statistical model capability was observed by changing them in a various way. Default parameters values are the following: d_{lower} = 1 Å; d_{upper} = 13 Å; *L* = 12; *point density* = 10 points/Å^2; *vdW radius reduction factor* = 1.000. Consequently, we derived 12 autocorrelation vectors per molecule, computed at the 12 (*L* value) distances in the interval from 1 to 13 Å with a step width of 1 Å. We considered that the step width of 1 Å, derived from the partition in 12 intervals of the global distance 1–13 Å, was sufficient to describe in an accurate way the distribution of the MEP property in the molecular surface. The autocorrelation transformation produces a molecular descriptor which is a unique fingerprint of each molecule under consideration. Autocorrelation vector have been calculated by ADRIANACODE.[30]

2.8. Support Vector Machine (SVM)

Support Vector Machines (SVMs) are learning systems originated from Statistical Learning Theory, proposed by Vapnik.[45,46] Here SVMs are applied to solve function approximation problems (approximation of unknown target functions), by using a training set represented as pairs of examples, $T = \{(x_1, y_1), (x_2, y_2), \ldots, (x_i, y_i)\}$, where x_i is an input sample and y_i is the corresponding desired value, directly observed from the unknown function. Usually $x_i \in \mathbb{R}^n$, while if $y_i^{\in\{-1,+1\}}$ the learning problem is a binary classification problem, if $y_i \in \mathbb{R}$ the learning problem is a regression problem. In both cases, the aim of the learning system is to select from a set of functions, that is, the *hypothesis space*, a hypothesis $f_{\text{opt}}(x)$ that approximates the desired responses y_i over the data set in an optimal fashion, for example, minimizing some risk functional *R* which weights the cost of the approximation, given by a loss or cost function that measures the distance between y_i and $f(x)$, with the probability to observe the input–output couple (x_i, y_i). In particular, we would like the function $f(x)$ to be a reasonable estimate of the functional relation between input–output pairs (prediction or *generalization* property).

The linear SVM is based on: (i) linear hypotheses corresponding to separating hyperplanes, that is, $f(x) = w \cdot x + b = \sum_{i=1}^{n} w_i x_i + b$, where $\cdot$ is the dot product between vectors; (ii) the solution of a quadratic optimization problem that represents a tradeoff between the minimization of the empirical error, that is, the error over the training set, and the maximization of the smoothness of $f(x)$.[46,47] Non-linear versions of SVM can be obtained by the introduction of a kernel.[47] An example of kernel function is the Gaussian kernel $k(x_i, x_j) = e^{-\gamma \|x_i - x_j\|^2}$. Let elaborate about these issues, both for classification and regression problems, in the following.

Support Vector Classification: Binary classification is widely performed to discriminate a set of compounds in two classes. The standard formulation for SVM is derived by using the Hinge loss function and slack variables ξ_i:

$$\min_{w,b} \frac{1}{2}\|w\|^2 + C\sum_{i=1}^{n} \xi_i$$

$$\text{subject to}: \forall i \in \{1, \ldots, n\} y_i (w \cdot x + b) \geqslant 1 - \xi_i \text{ and } \xi_i \geqslant 0,$$

where we recall that $y_i^{\in\{-1,+1\}}$, *w* and *b* are the parameters that control the function $f(x)$, and the constraints are satisfied with zero error when it is possible to find a function which is able to 'classify' any positive example (y_i = +1) by returning a positive value, that is, $f(x) \geqslant 1$, and any negative example (y_i = −1) returning a negative value, that is, $f(x) \leqslant -1$. If such function does not exist, then errors need to be compensated by choosing non-zero values for the corresponding slack variables ξ_i. The tradeoff between the minimization of the norm of the weight vector and the empirical error is given by the constant *C*.

It turns out that the above quadratic constrained minimization problem can be more easily solved by resorting to the corresponding dual problem

$$\max_{\alpha} \sum_{i=1}^{n} \alpha_i - \frac{1}{2}\sum_{i,j=1}^{n} \alpha_i \alpha_j y_i y_j (x_i \cdot x_j)$$

$$\text{subject to}: \sum_{i,j=1}^{n} y_i \alpha_i = 0, \text{ and } \forall_i \in \{1, \ldots, n\}\ 0 \leqslant \alpha_i \leqslant C,$$

where α_i are called the dual variables. The input vectors x_i for which the corresponding dual variables satisfy $\alpha_i^o > 0$ are referred to as support vectors, where α^o is the optimal solution vector of the dual problem. Finally, the decision rule is given by sgn($f(x)$).

Non-linearity of the boundary separating positive from negative samples is achieved by projecting the input vector into a higher dimensional feature space. In this way the dot product $x_i \cdot x_j$ is replaced by a kernel function $k(x_i \cdot x_j)$ representing the dot product in the transformed space, that is, $k(x_i \cdot x_j) = \Phi(x_i) \cdot \Phi(x_j)$. The decision function takes the final form

$$f(x) = \text{sgn}\left(\sum_{i=1}^{n} \alpha_i y_i k(x_i, x) + b\right).$$

Support Vector Regression (SVR):[48] If the learning task is defined as a regression problem, then the mathematical formulation has to take into account approximation errors. A 'reasonable' approximation is defined by introducing the constraint that for each input x_i we should have $|\, y_i - f(x)_i \,| \leqslant \varepsilon$, where ε is a small positive constant representing the tolerance we allow on approximation errors. This requirement can be represented by two linear constraints, that is, $(y_i - w \cdot x_i - b) \leqslant \varepsilon$ and $(w \cdot x_i + b - y_i) \leqslant \varepsilon$. Errors above the tolerance are typically linearly penalized by resorting to the linear ε-insensitive loss function, defined in the following way

$$L^{\varepsilon}(x, y, f) = |y - f(x)|_{\varepsilon} = \max(0, |y - f(x)| - \varepsilon).$$

On the basis of the above considerations, the standard SVR model is defined as

$$\min_{w,b,\xi_i,\xi_i^*} \frac{1}{2}\|w\|^2 + C\sum_{i=1}^{n}(\xi_i + \xi_i^*),$$

$$\text{subject to}: \forall i \in \{1, \ldots, n\}$$

$$(\langle w \cdot x_i \rangle + b) - y_i \leqslant \varepsilon + \xi_i,$$

$$y_i - (\langle w \cdot x_i \rangle + b) \leqslant \varepsilon + \xi_i^*,$$

$$\xi_i, \xi_i^* \geqslant 0,$$

where a set of slack variables ξ_i, ξ_i^*, is added to quantify the violation of the imposed constrains: ξ_i account for underestimation of the target values, while ξ_i^* account for overestimation of the target values. Note that, the solution of a linear regression problem results to be a tube with radius ε which approximates the data distribution.[45–48]

Even for SVR a kernel can be used to introduce non-linearity. In that case, the kernel expansion of the decision function *f* is

$$f(x, \alpha_i^*, \alpha_i) = \sum_{i=1}^{n} (\alpha_i^* - \alpha_i) k(x_i, x) + b.$$

The solution of the regression problem is a weighted sum of the kernel function evaluated at the support vectors, defined as the training points located on the border of the regression tube.

2.9. Classification model validation and evaluation

An extensive *n*-fold validation procedure was applied to evaluate the prediction capability of the SVM classification model (*auto*-MEP/SVM*class*). In particular leave-one-out, 10- and 5-fold cross-validation were performed for model validation. The average, standard deviation, minimum and maximum rates were collected for each *n*-fold cross-validation method. Then, the confusion matrix was extracted by comparing the experimental and predicted classes after LOO cross-validation and the test set prediction to confirm the robustness of our model. In the specific case, $hA_{2A}R$ antagonists are positive samples, while hA_3R antagonists are the negatives. The percentage (%) of correct predictions, sensitivity and specificity were calculated from the confusion matrix in the following way:

$$\text{Correct predictions } (\%) = \frac{TP + TN}{n},$$

$$\text{Sensitivity} = \frac{TP}{TP + FN},$$

$$\text{Specificity} = \frac{TN}{TN + FP}$$

where *TP* is the number of true positives, *TN* is the number of true negatives, *FP* are the false positives, *FN* are the false negatives and *n* is the total number of compounds. High percentage (%) values of correct predictions, sensitivity and specificity correspond to good modeling performances.

3. Chemistry

The desired compounds (**138–188**) have been prepared by acylation with the appropriate arylacetyl chloride (1.3 equiv) of the well-known and previously reported unsubstituted derivatives **45, 47, 51, 57–60** in dry THF at reflux (18 h) in the presence of triethylamine (1.3 equiv). See Scheme 1. When not commercially available the acyl chlorides were prepared from the corresponding acid by treatment with thionyl chloride in the presence of a catalytic amount of dimethyl formamide.

3.1. General

Reactions were routinely monitored by thin-layer chromatography (TLC) on silica gel (precoated F_{254} Merck plates). Infrared spectra (IR) were measured on a Jasco FT-IT instrument. ^{1}H NMR were determined in $CDCl_3$ or DMSO-d_6 solutions with a Varian Gemini 200 spectrometer, peaks positions are given in parts per million (δ) downfield from tetramethylsilane as internal standard, and *J* values are given in hertz. Light petroleum ether refers to the fractions boiling at 40–60 °C. Melting points were determined on a Buchi-Tottoli instrument and are uncorrected. Flash chromatography was performed using Merck 60–200 mesh silica gel. Elemental analyses were performed by the microanalytical laboratory of Dipartimento di Chimica, University of Trieste, and were within ±0.4% of the theoretical values for C, H and N. See Supplementary data for details.

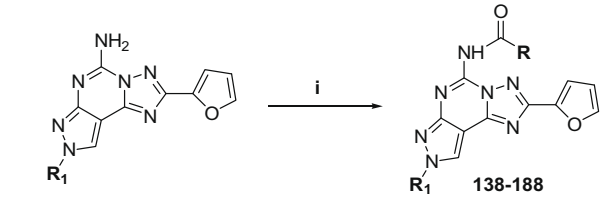

$R_1 = CH_3$, **45**; $R_1 = C_2H_5$, **57**;
$R_1 = nC_3H_7$, **58**; $R_1 = nC_4H_9$, **47**;
$R_1 = CH_2CH_2CH(CH_3)_2$, **51**;
$R_1 = CH_2CH_2Ph$, **59**;
$R_1 = CH_2CH_2CH_2Ph$, **60**

Scheme 1. Reagents and conditions: (i) RCOCl, TEA, THF, reflux, 18 h.

3.1.1. General procedures for the preparation of 5-[(aryl)carbonyl]amino-8-(ar)alkyl-2-(2-furyl)-pyrazolo[4,3-*e*] 1,2,4-triazolo[1,5-*c*] pyrimidine (138–188)

Amino compound (**45, 47, 51, 57–60**, 10 mmol) was dissolved in freshly distilled THF (15 ml) and appropriate acid chloride (13 mmol) and triethylamine (13 mmol) were added. The mixture was refluxed under argon for 18 h. Then the solvent was removed under reduced pressure and the residue was dissolved in EtOAc (30 ml) and washed twice with water (15 ml). The organic phase was dried on Na_2SO_4 and concentrated under reduced pressure. The residue was purified by flash chromatography (EtOAc–light petroleum 4:6) to afford the desired compounds (**138–188**).

3.1.1.1. 5-[(Diphenylmethyl)carbonyl]amino-8-methyl-2-(2-furyl)-pyrazolo[4,3-*e*]1,2,4-triazolo[1,5-*c*]pyrimidine (139). Yield 85%, white solid; mp 253 °C (EtOAc–light petroleum); IR (KBr): 3240–2975, 1680, 1615, 1590, 1515 cm^{-1}; ^{1}H NMR ($CDCl_3$) δ: 4.01 (s, 3H); 5.62 (s, 1 h); 6.71 (dd, 1H, *J* = 2, *J* = 4); 7.04–7.43 (m, 11H); 7.98 (d, 1H, *J* = 2); 8.79 (s, 1H); 11.38 (br s, 1H). MW 449.16. Anal. Calcd for $C_{25}H_{19}N_7O_2$: C, 66.81; H, 4.26; N, 21.81. Found: C, 66.25; H, 4.19; N, 22.01.

3.1.1.2. 5-[(4-Biphenylmethyl)carbonyl]amino-8-methyl-2-(2-furyl)-pyrazolo[4,3-*e*]1,2,4-triazolo[1,5-*c*]pyrimidine (140). Yield 77%, pale yellow solid; mp 256 °C (EtOAc–light petroleum); IR (KBr): 3230–2980, 1675, 1620, 1585, 1510 cm^{-1}; ^{1}H NMR ($CDCl_3$) δ: 4.01 (s, 2H); 4.19 (s, 3H); 6.70 (dd, 1H, *J* = 2, *J* = 4); 7.21 (d, 1H, *J* = 4); 7.25–7.48 (m, 5H); 7.59–7.71 (m, 4H); 7.96 (d, 1H, *J* = 2); 8.79 (s, 1H); 10.96 (br s, 1H). MW 449.16. Anal. Calcd for $C_{25}H_{19}N_7O_2$: C, 66.81; H, 4.26; N, 21.81. Found: C, 66.43; H, 4.21; N, 21.77.

3.1.1.3. 5-[(3-Chlorobenzyl)carbonyl]amino-8-methyl-2-(2-furyl)-pyrazolo[4,3-*e*]1,2,4-triazolo[1,5-*c*]pyrimidine (147). Yield 91%, yellow solid; mp 212 °C (EtOAc–light petroleum); IR (KBr): 3235–2975, 1678, 1617, 1588, 1510 cm^{-1}; ^{1}H NMR ($CDCl_3$) δ: 4.00 (s, 2H); 4.17 (s, 3H); 6.73 (dd, 1H, *J* = 2, *J* = 4); 7.20 (d, 1H, *J* = 4); 7.23–7.38 (m, 3H); 7.43 (s, 1H); 7.99 (d, 1H, *J* = 2); 8.80 (s, 1H); 11.15 (br s, 1H). MW 407.81. Anal. Calcd for $C_{19}H_{14}N_7O_2Cl$: C, 55.96; H, 3.46; N, 24.04. Found: C, 55.78; H, 3.39; N, 24.01.

3.1.1.4. 5-[(4-Chlorobenzyl)carbonyl]amino-8-methyl-2-(2-furyl)-pyrazolo[4,3-*e*]1,2,4-triazolo[1,5-*c*]pyrimidine (150). Yield 95%, brown solid; mp 165 °C (EtOAc–light petroleum); IR (KBr): 3230–2978, 1675, 1614, 1584, 1500 cm^{-1}; ^{1}H NMR ($CDCl_3$) δ: 4.15 (s, 3H); 5.03 (s, 2H); 6.67 (dd, 1H, *J* = 2, *J* = 4); 7.01 (d, 2H, *J* = 9); 7.20 (d, 1H, *J* = 4); 7.38 (d, 2H, *J* = 9); 7.97 (d, 1H, *J* = 2); 8.79 (s, 1H); 11.04 (br s, 1H). MW 407.81. Anal. Calcd for $C_{19}H_{14}N_7O_2Cl$: C, 55.96; H, 3.46; N, 24.04. Found: C, 56.12; H, 3.29; N, 24.19.

3.1.1.5. 5-[(4-Methoxybenzyl)carbonyl]amino-8-methyl-2-(2-furyl)-pyrazolo[4,3-*e*]1,2,4-triazolo[1,5-*c*]pyrimidine (152). Yield 83%, yellow solid; mp 212 °C (EtOAc–light petroleum); IR (KBr): 3227–2983, 1673, 1610, 1582, 1505 cm^{-1}; ^{1}H NMR ($CDCl_3$) δ: 3.62 (s, 3H); 3.85 (s, 2H); 4.12 (s, 3H); 6.64 (dd, 1H, *J* = 2, *J* = 4); 6.88 (d, 2H, *J* = 9); 7.19 (d, 1H, *J* = 4); 7.24 (d, 2H, *J* = 9); 7.99 (d, 1H, *J* = 2);

8.80 (s, 1H); 10.96 (br s, 1H). MW 403.39. Anal. Calcd for $C_{20}H_{17}N_7O_3$: C, 59.55; H, 4.25; N, 24.31. Found: C, 59.47; H, 4.12; N, 24.16.

3.1.1.6. 5-[(2-Thienylmethyl)carbonyl]amino-8-methyl-2-(2-furyl)-pyrazolo[4,3-*e*]1,2,4-triazolo[1,5-*c*]pyrimidine (161). Yield 68%, brown solid; mp 210 °C (EtOAc–light petroleum); IR (KBr): 3230–2985, 1670, 1615, 1587, 1515 cm^{-1}; ^1H NMR ($CDCl_3$) δ: 4.16 (s, 3H); 4.22 (s, 2H); 6.66 (dd, 1H, $J = 2$, $J = 4$); 7.01 (dd, 1H, $J = 2$, $J = 4$); 7.07 (d, 1H, $J = 2$); 7.21 (d, 1H, $J = 4$); 7.44 (d, 1H, $J = 4$); 7.97 (d, 1H, $J = 2$); 8.81 (s, 1H); 11.03 (br s, 1H). MW 379.40. Anal. Calcd for $C_{17}H_{13}N_7O_2S$: C, 53.82; H, 3.45; N, 25.84. Found: C, 54.03; H, 3.52; N, 25.88.

3.1.1.7. 5-[(3-Thienylmethyl)carbonyl]amino-8-methyl-2-(2-furyl)-pyrazolo[4,3-*e*]1,2,4-triazolo[1,5-*c*]pyrimidine (162). Yield 71%, brown solid; mp 200 °C (EtOAc–light petroleum); IR (KBr): 3234–2990, 1668, 1613, 1578, 1512 cm^{-1}; ^1H NMR ($CDCl_3$) δ: 4.02 (s, 2H); 4.16 (s, 3H); 6.69 (dd, 1H, $J = 2$, $J = 4$); 7.07 (d, 1H, $J = 4$); 7.23 (d, 1H, $J = 4$); 7.41 (s, 1H); 7.43 (d, 1H, $J = 4$); 7.98 (d, 1H, $J = 2$); 8.80 (s, 1H); 10.99 (br s, 1H). MW 379.40. Anal. Calcd for $C_{17}H_{13}N_7O_2S$: C, 53.82; H, 3.45; N, 25.84. Found: C, 53.66; H, 3.38; N, 25.70.

3.1.1.8. 5-[(β-Naphthylmethyl)carbonyl]amino-8-methyl-2-(2-furyl)-pyrazolo[4,3-*e*]1,2,4-triazolo[1,5-*c*]pyrimidine (163). Yield 87%, yellow solid; mp 209 °C (EtOAc–light petroleum); IR (KBr): 3250–2977, 1682, 1615, 1590, 1500 cm^{-1}; ^1H NMR ($CDCl_3$) δ: 4.15 (s, 3H); 4.19 (s, 2H); 6.62 (dd, 1H, $J = 2$, $J = 4$); 7.20 (d, 1H, $J = 4$); 7.39–7.58 (m, 3H); 7.68–7.89 (m, 4H); 7.99 (d, 1H, $J = 4$); 8.79 (s, 1H); 11.01 (br s, 1H). MW 423.43. Anal. Calcd for $C_{23}H_{17}N_7O_2$: C, 65.24; H, 4.05; N, 23.16. Found: C, 64.98; H, 4.01; N, 22.99.

3.1.1.9. 5-[(α-Naphthylmethyl)carbonyl]amino-8-methyl-2-(2-furyl)-pyrazolo[4,3-*e*]1,2,4-triazolo[1,5-*c*]pyrimidine (164). Yield 87%, pale yellow solid; mp 205 °C (EtOAc–light petroleum); IR (KBr): 3240–2985, 1675, 1613, 1584, 1511 cm^{-1}; ^1H NMR ($CDCl_3$) δ: 4.13 (s, 3H); 4.42 (s, 2H); 6.63 (dd, 1H, $J = 2$, $J = 4$); 7.19 (d, 1H, $J = 4$); 7.40–7.61 (m, 4H); 7.75–7.85 (m, 3H); 7.98 (d, 1H, $J = 4$); 8.78 (s, 1H); 11.08 (br s, 1H). MW 423.43. Anal. Calcd for $C_{23}H_{17}N_7O_2$: C, 65.24; H, 4.05; N, 23.16. Found: C, 65.38; H, 4.04; N, 23.22.

3.1.1.10. 5-[(4-Trifluorobenzyl)carbonyl]amino-8-methyl-2-(2-furyl)-pyrazolo[4,3-*e*]1,2,4-triazolo[1,5-*c*]pyrimidine (168). Yield 97%, pale yellow solid; mp 212 °C (EtOAc–light petroleum); IR (KBr): 3225–2980, 1670, 1613, 1580, 1505 cm^{-1}; ^1H NMR ($CDCl_3$) δ: 4.08 (s, 2H); 4.12 (s, 3H); 6.68 (dd, 1H, $J = 2$, $J = 4$); 7.21 (d, 1H, $J = 4$); 7.61 (d, 2H, $J = 9$); 7.74 (d, 2H, $J = 9$); 7.97 (d, 1H, $J = 2$); 8.80 (s, 1H); 11.19 (br s, 1H). MW 441.37. Anal. Calcd for $C_{20}H_{14}N_7O_2F_3$: C, 54.43; H, 3.20; N, 22.21. Found: C, 54.71; H, 3.28; N, 22.38.

3.1.1.11. 5-[(4-Chlorophenoxymethyl)carbonyl]amino-8-methyl-2-(2-furyl)-pyrazolo[4,3-*e*]1,2,4-triazolo[1,5-*c*]pyrimidine (171). Yield 83%, brown solid; mp 145 °C (EtOAc–light petroleum); IR (KBr): 3230–2980, 1670, 1615, 1590, 1515 cm^{-1}; ^1H NMR ($CDCl_3$) δ: 4.28 (s, 3H); 5.03 (s, 2H); 6.63 (dd, 1H, $J = 2$, $J = 4$); 7.01 (d, 2H, $J = 9$); 7.18 (d, 1H, $J = 4$); 7.31 (d, 2H, $J = 9$); 7.98 (d, 1H, $J = 2$); 8.78 (s, 1H); 11.03 (br s, 1H). MW 423.81. Anal. Calcd for $C_{19}H_{14}N_7O_3Cl$: C, 53.85; H, 3.33; N, 23.13. Found: C, 54.02; H, 3.37; N, 23.19.

3.1.1.12. 5-[(4-Fluorobenzyl)carbonyl]amino-8-methyl-2-(2-furyl)-pyrazolo[4,3-*e*]1,2,4-triazolo[1,5-*c*]pyrimidine (177). Yield 86%, brown solid; mp 192 °C (EtOAc–light petroleum); IR (KBr): 3232–2986, 1673, 1616, 1590, 1511 cm^{-1}; ^1H NMR ($CDCl_3$) δ: 4.01 (s, 2H); 4.18 (s, 3H); 6.66 (dd, 1H, $J = 2$, $J = 4$); 7.21 (d, 1H, $J = 4$); 7.23 (d, 2H, $J = 9$); 7.41 (d, 2H, $J = 9$); 7.98 (d, 1H, $J = 2$); 8.81 (s, 1H); 11.00 (br s, 1H). MW 391.36. Anal. Calcd for $C_{19}H_{14}N_7O_2F$: C, 58.31; H, 3.61; N, 25.05. Found: C, 58.07; H, 3.62; N, 24.96.

3.1.1.13. 5-[(2,6-Dichlorobenzyl)carbonyl]amino-8-methyl-2-(2-furyl)-pyrazolo[4,3-*e*]1,2,4-triazolo[1,5-*c*]pyrimidine (179). Yield 70%, yellow solid; mp 170 °C (EtOAc–light petroleum); IR (KBr): 3228–2983, 1675, 1614, 1591, 1513 cm^{-1}; ^1H NMR ($CDCl_3$) δ: 4.08 (s, 2H); 4.15 (s, 3H); 6.69 (dd, 1H, $J = 2$, $J = 4$); 7.20 (d, 1H, $J = 4$); 7.31–7.59 (m, 3H); 7.99 (d, 1H, $J = 2$); 8.84 (s, 1H); 11.15 (br s, 1H). MW 442.26. Anal. Calcd for $C_{19}H_{13}N_7O_2Cl_2$: C, 51.60; H, 2.96; N, 22.17. Found: C, 51.32; H, 3.00; N, 22.23.

3.1.1.14. 5-[(4-Biphenylmethyl)carbonyl]amino-8-ethyl-2-(2-furyl)-pyrazolo[4,3-*e*]1,2,4-triazolo[1,5-*c*]pyrimidine (151). Yield 72%, pale yellow solid; mp 105 °C (EtOAc–light petroleum); IR (KBr): 3226–2975, 1673, 1610, 1580, 1510 cm^{-1}; ^1H NMR ($CDCl_3$) δ: 1. 44 (t, 3H, $J = 6.7$), 4.01 (s, 2H); 4.40 (q, 2H, $J = 6.7$); 6.72 (dd, 1H, $J = 2$, $J = 4$); 7.19 (d, 1H, $J = 4$); 7.22–7.58 (m, 5H); 7.62–7.81 (m, 4H); 7.97 (d, 1H, $J = 2$); 8.79 (s, 1H); 10.96 (br s, 1H). MW 463.49. Anal. Calcd for $C_{26}H_{21}N_7O_2$: C, 67.38; H, 4.57; N, 21.15. Found: C, 66.99; H, 4.49; N, 21.08.

3.1.1.15. 5-[(2-Thienylmethyl)carbonyl]amino-8-ethyl-2-(2-furyl)-pyrazolo[4,3-*e*]1,2,4-triazolo[1,5-*c*]pyrimidine (160). Yield 65%, brown solid; mp 113 °C (EtOAc–light petroleum); IR (KBr): 3230–2985, 1670, 1618, 1589, 1512 cm^{-1}; ^1H NMR ($CDCl_3$) δ: 1.43 (t, 3H, $J = 6.7$); 4.21 (s, 2H); 4.43 (q, 2H, $J = 6.7$); 6.73 (dd, 1H, $J = 2$, $J = 4$); 7.00 (dd, 1H, $J = 2$, $J = 4$); 7.04 (d, 1H, $J = 2$); 7.20 (d, 1H, $J = 4$); 7.41 (d, 1H, $J = 4$); 7.99 (d, 1H, $J = 2$); 8.91 (s, 1H); 11.05 (br s, 1H). MW 393.42. Anal. Calcd for $C_{18}H_{15}N_7O_2S$: C, 54.95; H, 3.84; N, 24.92. Found: C, 55.11; H, 3.91; N, 24.79.

3.1.1.16. 5-[(3-Thienylmethyl)carbonyl]amino-8-ethyl-2-(2-furyl)-pyrazolo[4,3-*e*]1,2,4-triazolo[1,5-*c*]pyrimidine (159). Yield 68%, hygroscopic brown solid (EtOAc–light petroleum); IR (KBr): 3244–2991, 1674, 1615, 1590, 1514 cm^{-1}; ^1H NMR ($CDCl_3$) δ: 1.49 (t, 3H, $J = 6.7$); 4.40 (q, 2H, $J = 6.7$); 4.51 (s, 2H); 6.61 (dd, 1H, $J = 2$, $J = 4$); 7.00 (d, 1H, $J = 4$); 7.15 (d, 1H, $J = 4$); 7.35 (s, 1H); 7.45 (d, 1H, $J = 4$); 7.99 (d, 1H, $J = 2$); 8.82 (s, 1H); 10.35 (br s, 1H). MW 393.42. Anal. Calcd for $C_{18}H_{15}N_7O_2S$: C, 54.95; H, 3.84; N, 24.92. Found: C, 54.68; H, 3.79; N, 24.77.

3.1.1.17. 5-[(β-Naphthylmethyl)carbonyl]amino-8-ethyl-2-(2-furyl)-pyrazolo[4,3-*e*]1,2,4-triazolo[1,5-*c*]pyrimidine (158). Yield 91%, pale yellow solid; mp 97 °C (EtOAc–light petroleum); IR (KBr): 3235–2987, 1676, 1620, 1587, 1505 cm^{-1}; ^1H NMR ($CDCl_3$) δ: 1.47 (t, 3H, $J = 6.7$); 4.18 (s, 2H); 4.41 (q, 2H, $J = 6.7$); 6.78 (dd, 1H, $J = 2$, $J = 4$); 7.21 (d, 1H, $J = 4$); 7.36–7.60 (m, 3H); 7.77–7.99 (m, 4H); 8.01 (d, 1H, $J = 4$); 8.83 (s, 1H); 11.05 (br s, 1H). MW 437.45. Anal. Calcd for $C_{24}H_{19}N_7O_2$: C, 65.89; H, 4.38; N, 22.41. Found: C, 65.66; H, 4.37; N, 22.29.

3.1.1.18. 5-[(α-Naphthylmethyl)carbonyl]amino-8-ethyl-2-(2-furyl)-pyrazolo[4,3-*e*]1,2,4-triazolo[1,5-*c*]pyrimidine (157). Yield 90%, pale yellow solid; mp 135 °C (EtOAc–light petroleum); IR (KBr): 3238–2980, 1676, 1611, 1580, 1500 cm^{-1}; ^1H NMR ($CDCl_3$) δ: 1.46 (t, 3H, $J = 6.7$); 4.41 (q, 2H, $J = 6.7$); 4.53 (s, 2H); 6.67 (dd, 1H, $J = 2$, $J = 4$); 7.20 (d, 1H, $J = 4$); 7.41–7.64 (m, 4H); 7.79–7.99 (m, 3H); 8.01 (d, 1H, $J = 4$); 8.84 (s, 1H); 11.05 (br s, 1H). MW 437.45. Anal. Calcd for $C_{24}H_{19}N_7O_2$: C, 65.89; H, 4.38; N, 22.41. Found: C, 66.02; H, 4.42; N, 22.53.

3.1.1.19. 5-[(Diphenylmethyl)carbonyl]amino-8-*n*-propyl-2-(2-furyl)-pyrazolo[4,3-*e*]1,2,4-triazolo[1,5-*c*]pyrimidine (148). Yield 85%, white solid; mp 212 °C (EtOAc–light petroleum); IR (KBr): 3235–2980, 1673, 1610, 1592, 1510 cm^{-1}; ^1H NMR ($CDCl_3$) δ: 0.91 (t, 3H, $J = 6.7$), 1.81–1.99 (m, 2H); 4.39 (t, 2H, $J = 6.7$); 5.61 (s, 1H); 6.67 (dd, 1H, $J = 2$, $J = 4$); 7.08–7.58 (m, 11H); 7.99 (d, 1H, $J = 2$); 8.81 (s, 1H); 11.35 (br s, 1H). MW 477.52. Anal. Calcd for $C_{27}H_{23}N_7O_2$: C, 67.91; H, 4.85; N, 20.53. Found: C, 67.69; H, 4.77; N, 20.42.

3.1.1.20. 5-[(4-Biphenylmethyl)carbonyl]amino-8-*n*-propyl-2-(2-furyl)-pyrazolo[4,3-*e*]1,2,4-triazolo[1,5-*c*]pyrimidine (149). Yield 79%, pale yellow solid; mp 218 °C (EtOAc–light petroleum); IR (KBr): 3235–2985, 1676, 1620, 1587, 1500 cm^{-1}; ^1H NMR ($CDCl_3$) δ: 0.93 (t, 3H, J = 6.7), 1.83–1.94 (m, 2H); 4.01 (s, 2H); 4.37 (t, 2H, J = 6.7); 6.76 (dd, 1H, J = 2, J = 4); 7.20 (d, 1H, J = 4); 7.25–7.59 (m, 5H); 7.61–7.79 (m, 4H); 7.98 (d, 1H, J = 2); 8.81 (s, 1H); 11.03 (br s, 1H). MW 477.52. Anal. Calcd for $C_{27}H_{23}N_7O_2$: C, 67.91; H, 4.85; N, 20.53. Found: C, 68.01; H, 4.86; N, 20.57.

3.1.1.21. 5-[(β-Naphthylmethyl)carbonyl]amino-8-*n*-propyl-2-(2-furyl)-pyrazolo[4,3-*e*]1,2,4-triazolo[1,5-*c*]pyrimidine (166). Yield 82%, pale yellow solid; mp 80 °C (EtOAc–light petroleum); IR (KBr): 3230–2980, 1680, 1615, 1584, 1515 cm^{-1}; ^1H NMR ($CDCl_3$) δ: 0.85 (t, 3H, J = 6.7), 1.80–2.01 (m, 2H); 4.19 (s, 2H); 4.35 (t, 2H, J = 6.7); 6.75 (dd, 1H, J = 2, J = 4); 7.23 (d, 1H, J = 4); 7.40–7.62 (m, 3H); 7.80–7.95 (m, 4H); 7.99 (d, 1H, J = 4); 8.81 (s, 1H); 11.07 (br s, 1H). MW 451.48. Anal. Calcd for $C_{25}H_{21}N_7O_2$: C, 66.51; H, 4.69; N, 21.72. Found: C, 66.23; H, 4.60; N, 21.80.

3.1.1.22. 5-[(α-Naphthylmethyl)carbonyl]amino-8-*n*-propyl-2-(2-furyl)-pyrazolo[4,3-*e*]1,2,4-triazolo[1,5-*c*]pyrimidine (165). Yield 75%, pale yellow solid; mp 170 °C (EtOAc–light petroleum); IR (KBr): 3230–2985, 1675, 1615, 1583, 1506 cm^{-1}; ^1H NMR ($CDCl_3$) δ: 0.85 (t, 3H, J = 6.7), 1.79–1.99 (m, 2H); 4.35 (t, 2H, J = 6.7); 4.53 (s, 2H); 6.77 (dd, 1H, J = 2, J = 4); 7.22 (d, 1H, J = 4); 7.40–7.63 (m, 4H); 7.79–8.00 (m, 3H); 8.03 (d, 1H, J = 4); 8.83 (s, 1H); 11.18 (br s, 1H). MW 451.48. Anal. Calcd for $C_{25}H_{21}N_7O_2$: C, 66.51; H, 4.69; N, 21.72. Found: C, 66.30; H, 4.73; N, 21.67.

3.1.1.23. 5-[(Diphenylmethyl)carbonyl]amino-8-*n*-butyl-2-(2-furyl)-pyrazolo[4,3-*e*]1,2,4-triazolo[1,5-*c*]pyrimidine (145). Yield 75%, white solid; mp 195 °C (EtOAc–light petroleum); IR (KBr): 3230–2985, 1672, 1615, 1600, 1520 cm^{-1}; ^1H NMR ($CDCl_3$) δ: 0.81 (t, 3H, J = 6.7), 1.01–1.28 (m, 2H); 1.78–1.99 (m, 2H); 4.38 (t, 2H, J = 6.7); 5.65 (s, 1H); 6.68 (dd, 1H, J = 2, J = 4); 7.04–7.55 (m, 11H); 7.98 (d, 1H, J = 2); 8.82 (s, 1H); 11.37 (br s, 1H). MW 491.54. Anal. Calcd for $C_{28}H_{25}N_7O_2$: C, 68.42; H, 5.13; N, 19.95. Found: C, 68.17; H, 5.08; N, 20.02.

3.1.1.24. 5-[(4-Biphenylmethyl)carbonyl]amino-8-*n*-butyl-2-(2-furyl)-pyrazolo[4,3-*e*]1,2,4-triazolo[1,5-*c*]pyrimidine (146). Yield 83%, pale yellow solid; mp 180 °C (EtOAc–light petroleum); IR (KBr): 3235–2985, 1676, 1620, 1587, 1500 cm^{-1}; ^1H NMR ($CDCl_3$) δ: 0.83 (t, 3H, J = 6.7), 1.05–1.25 (m, 2H); 1.69–1.99 (m, 2H); 4.00 (s, 2H); 4.39 (t, 2H, J = 6.7); 6.63 (dd, 1H, J = 2, J = 4); 7.18 (d, 1H, J = 4); 7.21–7.55 (m, 5H); 7.59–7.76 (m, 4H); 7.93 (d, 1H, J = 2); 8.81 (s, 1H); 11.00 (br s, 1H). MW 491.54. Anal. Calcd for $C_{28}H_{25}N_7O_2$: C, 68.42; H, 5.13; N, 19.95. Found: C, 68.63; H, 5.13; N, 20.05.

3.1.1.25. 5-[(2-Thienylmethyl)carbonyl]amino-8-*n*-butyl-2-(2-furyl)-pyrazolo[4,3-*e*]1,2,4-triazolo[1,5-*c*]pyrimidine (169). Yield 66%, hygroscopic brown solid; (EtOAc–light petroleum); IR (KBr): 3230–2975, 1675, 1610, 1580, 1515 cm^{-1}; ^1H NMR ($CDCl_3$) δ: 0.81 (t, 3H, J = 6.7), 1.08–1.35 (m, 2H); 1.68–2.00 (m, 2H); 4.21 (s, 2H); 4.37 (t, 2H, J = 6.7); 6.66 (dd, 1H, J = 2, J = 4); 6.99 (dd, 1H, J = 2, J = 4); 7.02 (d, 1H, J = 2); 7.22 (d, 1H, J = 4); 7.41 (d, 1H, J = 4); 7.98 (d, 1H, J = 2); 8.83 (s, 1H); 11.03 (br s, 1H). MW 421.48. Anal. Calcd for $C_{20}H_{19}N_7O_2S$: C, 56.99; H, 4.54; N, 23.26. Found: C, 57.19; H, 4.49; N, 23.31.

3.1.1.26. 5-[(3-Thienylmethyl)carbonyl]amino-8-*n*-butyl-2-(2-furyl)-pyrazolo[4,3-*e*]1,2,4-triazolo[1,5-*c*]pyrimidine (170). Yield 60%, hygroscopic brown solid (EtOAc–light petroleum); IR (KBr): 3230–2985, 1673, 1615, 1580, 1512 cm^{-1}; ^1H NMR ($CDCl_3$) δ: 0.83 (t, 3H, J = 6.7), 1.04–1.38 (m, 2H); 1.69–2.01 (m, 2H); 4.01 (s, 2H); 4.39 (t, 2H, J = 6.7); 6.75 (dd, 1H, J = 2, J = 4); 7.08 (d, 1H, J = 4); 7.21 (d, 1H, J = 4); 7.41 (s, 1H); 7.58 (d, 1H, J = 4); 7.99 (d, 1H, J = 2); 8.82 (s, 1H); 10.97 (br s, 1H). MW 421.48. Anal. Calcd for $C_{20}H_{19}N_7O_2S$: C, 56.99; H, 4.54; N, 23.26. Found: C, 56.69; H, 4.47; N, 23.19.

3.1.1.27. 5-[(α-Naphthylmethyl)carbonyl]amino-8-*n*-butyl-2-(2-furyl)-pyrazolo[4,3-*e*]1,2,4-triazolo[1,5-*c*]pyrimidine (167). Yield 75%, pale yellow solid; mp 95 °C (EtOAc–light petroleum); IR (KBr): 3227–2982, 1673, 1619, 1580, 1500 cm^{-1}; ^1H NMR ($CDCl_3$) δ: 0.85 (t, 3H, J = 6.7), 1.14–1.29 (m, 2H); 1.73–1.98 (m, 2H); 4.35 (t, 2H, J = 6.7); 4.49 (s, 2H); 6.73 (dd, 1H, J = 2, J = 4); 7.22 (d, 1H, J = 4); 7.39–7.61 (m, 4H); 7.78–8.00 (m, 3H); 8.01 (d, 1H, J = 4); 8.82 (s, 1H); 11.04 (br s, 1H). MW 465.51. Anal. Calcd for $C_{26}H_{23}N_7O_2$: C, 67.08; H, 4.98; N, 21.06. Found: C, 67.23; H, 4.95; N, 21.01.

3.1.1.28. 5-[(Diphenylmethyl)carbonyl]amino-8-isopentyl-2-(2-furyl)-pyrazolo[4,3-*e*]1,2,4-triazolo[1,5-*c*]pyrimidine (141). Yield 78%, white solid; mp 180 °C (EtOAc–light petroleum); IR (KBr): 3235–2980, 1677, 1618, 1585, 1505 cm^{-1}; ^1H NMR ($CDCl_3$) δ: 0.83 (d, 6H, J = 7); 1.35–1.45 (m, 1H); 1.71–1.81 (m, 2H); 4.38 (t, 2H. J = 6.7); 5.64 (s, 1H); 6.75 (dd, 1H, J = 2, J = 4); 7.14–7.45 (m, 11H); 7.97 (d, 1H, J = 2); 8.83 (s, 1H); 11.35 (br s, 1H). MW 465.51. Anal. Calcd for $C_{29}H_{27}N_7O_2$: C, 68.89; H, 5.38; N, 19.39. Found: C, 68.57; H, 5.23; N, 19.48.

3.1.1.29. 5-[(4-Biphenylmethyl)carbonyl]amino-8-isopentyl-2-(2-furyl)-pyrazolo[4,3-*e*]1,2,4-triazolo[1,5-*c*]pyrimidine (142). Yield 74%, pale yellow solid; mp 130 °C (EtOAc–light petroleum); IR (KBr): 3225–2975, 1672, 1610, 1575, 1513 cm^{-1}; ^1H NMR ($CDCl_3$) δ: 0.84 (d, 6H, J = 7); 1.38–1.57 (m, 1H); 1.70–1.82 (m, 2H); 4.01 (s, 2H); 4.40 (t, 2H. J = 6.7); 6.72 (dd, 1H, J = 2, J = 4); 7.21 (d, 1H, J = 4); 7.26–7.51 (m, 5H); 7.57–7.69 (m, 4H); 7.97 (d, 1H, J = 2); 8.82 (s, 1H); 11.03 (br s, 1H). MW 465.51. Anal. Calcd for $C_{29}H_{27}N_7O_2$: C, 68.89; H, 5.38; N, 19.39. Found: C, 68.63; H, 5.31; N, 19.43.

3.1.1.30. 5-[(3-Chlorobenzyl)carbonyl]amino-8-isopentyl-2-(2-furyl)-pyrazolo[4,3-*e*]1,2,4-triazolo[1,5-*c*]pyrimidine (172). Yield 89%, pale yellow solid; mp 95 °C (EtOAc–light petroleum); IR (KBr): 3235–2987, 1676, 1610, 1580, 1500 cm^{-1}; ^1H NMR ($CDCl_3$) δ: 0.83 (d, 6H, J = 7); 1.35–1.55 (m, 1H); 1.69–1.80 (m, 2H); 4.04 (s, 2H); 4.40 (t, 2H. J = 6.7); 6.69 (dd, 1H, J = 2, J = 4); 7.19 (d, 1H, J = 4); 7.22–7.34 (m, 3H); 7.44 (s, 1H); 8.00 (d, 1H, J = 2); 8.78 (s, 1H); 11.05 (br s, 1H). MW 463.92. Anal. Calcd for $C_{23}H_{22}N_7O_2Cl$: C, 59.55; H, 4.78; N, 21.13. Found: C, 59.27; H, 4.59; N, 21.10.

3.1.1.31. 5-[(4-Chlorobenzyl)carbonyl]amino-8-isopentyl-2-(2-furyl)-pyrazolo[4,3-*e*]1,2,4-triazolo[1,5-*c*]pyrimidine (173). Yield 86%, white solid; mp 92 °C (EtOAc–light petroleum); IR (KBr): 3225–2975, 1672, 1610, 1590, 1507 cm^{-1}; ^1H NMR ($CDCl_3$) δ: 0.85 (d, 6H, J = 7); 1.36–1.55 (m, 1H); 1.66–1.81 (m, 2H); 4.38 (t, 2H. J = 6.7); 5.01 (s, 2H); 6.68 (dd, 1H, J = 2, J = 4); 7.01 (d, 2H, J = 9); 7.19 (d, 1H, J = 4); 7.37 (d, 2H, J = 9); 7.99 (d, 1H, J = 2); 8.90 (s, 1H); 11.15 (br s, 1H). MW 463.92. Anal. Calcd for $C_{23}H_{22}N_7O_2Cl$: C, 59.55; H, 4.78; N, 21.13. Found: C, 59.83; H, 4.81; N, 21.09.

3.1.1.32. 5-[(β-Naphthylmethyl)carbonyl]amino-8-isopentyl-2-(2-furyl)-pyrazolo[4,3-*e*]1,2,4-triazolo[1,5-*c*]pyrimidine (153). Yield 80%, yellow solid; mp 180 °C (EtOAc–light petroleum); IR (KBr): 3225–2970, 1676, 1610, 1584, 1505 cm^{-1}; ^1H NMR ($CDCl_3$) δ: 0.84 (d, 6H, J = 7); 1.30–1.57 (m, 1H); 1.69–1.81 (m, 2H); 4.21 (s, 2H); 4.41 (t, 2H. J = 6.7); 6.68 (dd, 1H, J = 2, J = 4); 7.19 (d, 1H, J = 4); 7.36–7.55 (m, 3H); 7.67–7.89 (m, 4H); 7.98 (d, 1H, J = 4); 8.81 (s, 1H); 11.08 (br s, 1H). MW 479.53. Anal. Calcd for $C_{27}H_{25}N_7O_2$: C, 67.63; H, 5.25; N, 20.45. Found: C, 67.30; H, 5.18; N, 20.29.

3.1.1.33. 5-[(4-Trifluorobenzyl)carbonyl]amino-8-isopentyl-2-(2-furyl)-pyrazolo[4,3-*e*]1,2,4-triazolo[1,5-*c*]pyrimidine (175). Yield 97%, pale yellow solid; mp 95 °C (EtOAc–light petroleum); IR (KBr): 3230–2984, 1684, 1620, 1575, 1512 cm^{-1}; ^1H NMR ($CDCl_3$) δ: 0.86 (d, 6H, J = 7); 1.38–1.57 (m, 1H); 1.67–1.83 (m, 2H); 4.13 (s, 2H); 4.39 (t, 2H. J = 6.7); 6.66 (dd, 1H, J = 2, J = 4); 7.20 (d, 1H, J = 4); 7.61 (d, 2H, J = 9); 7.72 (d, 2H, J = 9); 7.99 (d, 1H, J = 2); 8.82 (s, 1H); 11.01 (br s, 1H). MW 497.47. Anal. Calcd for $C_{24}H_{22}N_7O_2F_3$: C, 57.94; H, 4.46; N, 19.71. Found: C, 58.07; H, 4.45; N, 19.84.

3.1.1.34. 5-[(4-Fluorobenzyl)carbonyl]amino-8-methyl-2-(2-furyl)-pyrazolo[4,3-*e*]1,2,4-triazolo[1,5-*c*]pyrimidine (176). Yield 90%, pale yellow solid; mp 133 °C (EtOAc–light petroleum); IR (KBr): 3235–2990, 1680, 1610, 1585, 1510 cm^{-1}; ^1H NMR ($CDCl_3$) δ: 0.82 (d, 6H, J = 7); 1.31–1.54 (m, 1H); 1.66–1.83 (m, 2H); 3.99 (s, 2H); 4.39 (t, 2H. J = 6.7); 6.68 (dd, 1H, J = 2, J = 4); 7.14 (d, 1H, J = 4); 7.19 (d, 2H, J = 9); 7.37 (d, 2H, J = 9); 7.95 (d, 1H, J = 2); 8.86 (s, 1H); 11.02 (br s, 1H). MW 447.46. Anal. Calcd for $C_{23}H_{22}N_7O_2F$: C, 61.74; H, 4.96; N, 21.91. Found: C, 61.96; H, 4.79; N, 22.05.

3.1.1.35. 5-[(2,6-Dichlorobenzyl)carbonyl]amino-8-isopentyl-2-(2-furyl)-pyrazolo[4,3-*e*]1,2,4-triazolo[1,5-*c*]pyrimidine (178). Yield 70%, white solid; mp 130 °C (EtOAc–light petroleum); IR (KBr): 3225–2975, 1677, 1615, 1580, 1506 cm^{-1}; ^1H NMR ($CDCl_3$) δ: 0.86 (d, 6H, J = 7); 1.33–1.56 (m, 1H); 1.71–1.85 (m, 2H); 4.37 (s, 2H); 4.39 (t, 2H. J = 6.7); 6.67 (dd, 1H, J = 2, J = 4); 7.19 (d, 1H, J = 4); 7.29–7.57 (m, 3H); 8.01 (d, 1H, J = 2); 8.80 (s, 1H); 11.03 (br s, 1H). MW 447.46. Anal. Calcd for $C_{23}H_{21}N_7O_2Cl_2$: C, 55.10; H, 4.82; N, 19.56. Found: C, 54.95; H, 4.77; N, 19.63.

3.1.1.36. 5-[(Diphenylmethyl)carbonyl]amino-8-(2-phenylethyl)-2-(2-furyl)-pyrazolo[4,3-*e*]1,2,4-triazolo[1,5-*c*]pyrimidine (143). Yield 94%, white solid; mp 109 °C (EtOAc–light petroleum); IR (KBr): 3215–2970, 1680, 1615, 1580, 1510 cm^{-1}; ^1H NMR ($CDCl_3$) δ: 3.46 (t, 2H, J = 7); 4.52 (t, 2H, J = 7); 5.60 (s, 1H); 6.71 (dd, 1H, J = 2, J = 4); 7.05–7.48 (m, 16H); 7.98 (d, 1H, J = 2); 8.80 (s, 1H); 11.28 (br s, 1H). MW 539.59. Anal. Calcd for $C_{32}H_{25}N_7O_2$: C, 71.23; H, 4.67; N, 18.17. Found: C, 70.95; H, 4.72; N, 18.21.

3.1.1.37. 5-[(4-Biphenylmethyl)carbonyl]amino-8-(2-phenylethyl)-2-(2-furyl)-pyrazolo[4,3-*e*]1,2,4-triazolo[1,5-*c*]pyrimidine (144). Yield 80%, pale yellow solid; mp 95 °C (EtOAc–light petroleum); IR (KBr): 3225–2975, 1678, 1615, 1580, 1510 cm^{-1}; ^1H NMR ($CDCl_3$) δ: 3.46 (t, 2H, J = 7); 4.01 (s, 2H); 4.52 (t, 2H, J = 7); 6.70 (dd, 1H, J = 2, J = 4); 7.06–7.69 (m, 15H); 7.96 (d, 1H, J = 2); 8.79 (s, 1H); 11.01 (br s, 1H). MW 539.59. Anal. Calcd for $C_{32}H_{25}N_7O_2$: C, 71.23; H, 4.67; N, 18.17. Found: C, 71.13; H, 4.55; N, 18.08.

3.1.1.38. 5-[(3-Chlorobenzyl)carbonyl]amino-8-(2-phenylethyl)-2-(2-furyl)-pyrazolo[4,3-*e*]1,2,4-triazolo[1,5-*c*]pyrimidine (174). Yield 89%, pale yellow solid; mp 83 °C (EtOAc–light petroleum); IR (KBr): 3235–2990, 1679, 1613, 1577, 1505 cm^{-1}; ^1H NMR ($CDCl_3$) δ: 3.48 (t, 2H, J = 7); 5.09 (s, 2H); 4.50 (t, 2H, J = 7); 6.78 (dd, 1H, J = 2, J = 4); 7.19 (d, 1H, J = 4); 7.21–7.40 (m, 9H); 7.99 (d, 1H, J = 2); 8.68 (s, 1H); 10.99 (br s, 1H). MW 497.94. Anal. Calcd for $C_{26}H_{20}N_7O_2Cl$: C, 62.71; H, 4.05; N, 19.69. Found: C, 62.34; H, 3.98; N, 19.47.

3.1.1.39. 5-[(2-Thienylmethyl)carbonyl]amino-8-(2-phenylethyl)-2-(2-furyl)-pyrazolo[4,3-*e*]1,2,4-triazolo[1,5-*c*] pyrimidine (155). Yield 71%, hygroscopic brown solid; (EtOAc–light petroleum); IR (KBr): 3220–2980, 1678, 1610, 1585, 1510 cm^{-1}; ^1H NMR ($CDCl_3$) δ: 3.43 (t, 2H, J = 7); 4.54 (t, 2H, J = 7); 4.71 (s, 2H); 6.69 (dd, 1H, J = 2, J = 4); 7.02–7.41 (m, 9H); 7.97 (d, 1H, J = 2); 8.78 (s, 1H); 10.11 (br s, 1H). MW 469.52. Anal. Calcd for $C_{24}H_{19}N_7O_2S$: C, 61.39; H, 4.08; N, 20.88. Found: C, 61.08; H, 4.13; N, 20.65.

3.1.1.40. 5-[(3-Thienylmethyl)carbonyl]amino-8-(2-phenylethyl)-2-(2-furyl)-pyrazolo[4,3-*e*]1,2,4-triazolo[1,5-*c*]pyrimidine (156). Yield 67%, hygroscopic brown solid; (EtOAc–light petroleum); IR (KBr): 3220–2980, 1675, 1610, 1580, 1512 cm^{-1}; ^1H NMR ($CDCl_3$) δ: 3.46 (t, 2H, J = 7); 4.45 (s, 2H); 4.52 (t, 2H, J = 7); 6.66 (dd, 1H, J = 2, J = 4); 7.01 7.39 (m, 9H); 7.98 (d, 1H, J = 2); 8.79 (s, 1H); 10.87 (br s, 1H). MW 469.52. Anal. Calcd for $C_{24}H_{19}N_7O_2S$: C, 61.39; H, 4.08; N, 20.88. Found: C, 61.65; H, 4.01; N, 20.57.

3.1.1.41. 5-[(β-Naphthylmethyl)carbonyl]amino-8-(2-phenylethyl)-2-(2-furyl)-pyrazolo[4,3-*e*]1,2,4-triazolo[1,5-*c*]pyrimidine (154). Yield 77%, white solid; mp 113 °C (EtOAc–light petroleum); IR (KBr): 3220–2970, 1681, 1610, 1575, 1510 cm^{-1}; ^1H NMR ($CDCl_3$) δ: 3.43 (t, 2H, J = 7); 4.40 (s, 2H); 4.61 (t, 2H, J = 7 Hz); 6.66 (dd, 1H, J = 2 Hz, J = 4 Hz); 7.07–7.14 (m, 5H); 7.23–7.36 (m, 4H); 7.83–7.99 (m, 4H); 8.02 (d, 1H, J = 4 Hz); 8.84 (s, 1H); 11.11 (br s, 1H). MW 513.55. Anal. Calcd for $C_{30}H_{23}N_7O_2$: C, 70.16; H, 4.51; N, 19.09. Found: C, 69.88; H, 4.43; N, 19.25.

3.1.1.42. 5-[(Diphenylmethyl)carbonyl]amino-8-(3-phenylpropyl)-2-(2-furyl)-pyrazolo[4,3-*e*]1,2,4-triazolo[1,5-*c*]pyrimidine (181). Yield 80%, pale yellow solid; mp 193 °C (EtOAc–light petroleum); IR (KBr): 3225–2980, 1677, 1610, 1595, 1515 cm^{-1}; ^1H NMR ($CDCl_3$) δ: 2.20 (t, 2H, J = 7); 2.55–2.65 (m, 2H); 4.41 (t, 2H, J = 7); 5.68 (s, 1H); 6.75 (dd, 1H, J = 2, J = 4); 7.01–7.57 (m, 16H); 7.99 (d, 1H, J = 2); 8.87 (s, 1H); 11.39 (br s, 1H). MW 553.61. Anal. Calcd for $C_{33}H_{27}N_7O_2$: C, 71.59; H, 4.92; N, 17.71. Found: C, 71.63; H, 5.01; N, 17.93.

3.1.1.43. 5-[(4-Biphenylmethyl)carbonyl]amino-8-(3-phenylpropyl)-2-(2-furyl)-pyrazolo[4,3-*e*]1,2,4-triazolo[1,5-*c*]pyrimidine (188). Yield 76%, yellow solid; mp 150 °C (EtOAc–light petroleum); IR (KBr): 3225–2980, 1674, 1610, 1575, 1515 cm^{-1}; ^1H NMR ($CDCl_3$) δ: 2.20 (t, 2H, J = 7); 2.55–2.65 (m, 2H); 4.41 (t, 2H, J = 7); 4.59 (s, 2H); 6.61 (dd, 1H, J = 2, J = 4); 7.00–7.73 (m, 15H); 8.17 (d, 1H, J = 2); 9.13 (s, 1H); 11.33 (br s, 1H). MW 553.61. Anal. Calcd for $C_{33}H_{27}N_7O_2$: C, 71.59; H, 4.92; N, 17.71. Found: C, 71.21; H, 4.86; N, 17.69.

3.1.1.44. 5-[(3-Chlorobenzyl)carbonyl]amino-8-(3-phenylpropyl)-2-(2-furyl)-pyrazolo[4,3-*e*]1,2,4-triazolo[1,5-*c*]pyrimidine (184). Yield 95%, white solid; mp 98 °C (EtOAc–light petroleum); IR (KBr): 3230–2985, 1675, 1610, 1580, 1508 cm^{-1}; ^1H NMR ($CDCl_3$) δ: 2.20 (t, 2H, J = 7); 2.55–2.65 (m, 2H); 4.01 (s, 2H); 4.41 (t, 2H, J = 7); 6.73 (dd, 1H, J = 2, J = 4); 7.02–7.61 (m, 10H); 7.96 (d, 1H, J = 2); 8.86 (s, 1H); 11.09 (br s, 1H). MW 511.96. Anal. Calcd for $C_{27}H_{22}N_7O_2Cl$: C, 63.34; H, 4.33; N, 19.15. Found: C, 63.07; H, 4.22; N, 19.01.

3.1.1.45. 5-[(4-Chlorobenzyl)carbonyl]amino-8-(3-phenylpropyl)-2-(2-furyl)-pyrazolo[4,3-*e*]1,2,4-triazolo[1,5-*c*]pyrimidine (185). Yield 78%, yellow solid; mp 101 °C (EtOAc–light petroleum); IR (KBr): 3225–2980, 1674, 1610, 1580, 1508 cm^{-1}; ^1H NMR ($CDCl_3$) δ: 2.22 (t, 2H, J = 7); 2.52–2.64 (m, 2H); 4.40 (t, 2H, J = 7); 4.53 (s, 2H); 6.60 (dd, 1H, J = 2, J = 4); 7.04–7.58 (m, 10H); 8.18 (d, 1H, J = 2); 9.10 (s, 1H); 11.05 (br s, 1H). MW 511.96. Anal. Calcd for $C_{27}H_{22}N_7O_2Cl$: C, 63.34; H, 4.33; N, 19.15. Found: C, 63.51; H, 4.34; N, 19.22.

3.1.1.46. 5-[(β-Naphthylmethyl)carbonyl]amino-8-(3-phenylpropyl)-2-(2-furyl)-pyrazolo[4,3-*e*]1,2,4-triazolo[1,5-*c*]pyrimidine (182). Yield 77%, white solid; mp 113 °C (EtOAc–light petroleum); IR (KBr): 3225–2980, 1679, 1610, 1580, 1510 cm^{-1};

^{1}H NMR ($CDCl_3$) δ: 2.21 (t, 2H, J = 7); 2.53–2.65 (m, 2H); 4.16 (s, 2H); 4.40 (t, 2H, J = 7); 6.68 (dd, 1H, J = 2 Hz, J = 4 Hz); 7.02–7.14 (m, 5H); 7.21–7.33 (m, 4H); 7.80–7.98 (m, 4H); 8.00 (d, 1H, J = 4 Hz); 8.86 (s, 1H); 11.07 (br s, 1H). MW 527.58. Anal. Calcd for $C_{30}H_{23}N_7O_2$: C, 70.57; H, 4.78; N, 18.58. Found: C, 70.30; H, 4.56; N, 18.74.

3.1.1.47. 5-[(4-Fluorobenzyl)carbonyl]amino-8-(3-phenylpropyl)-2-(2-furyl)-pyrazolo[4,3-*e*]1,2,4-triazolo[1,5-*c*]pyrimidine (180). Yield 75%, yellow solid; mp 90 °C (EtOAc–light petroleum); IR (KBr): 3230–2990, 1675, 1615, 1580, 1510 cm^{-1}; ^{1}H NMR ($CDCl_3$) δ: 2.23 (t, 2H, J = 7); 2.51–2.63 (m, 2H); 3.98 (s, 2H); 4.38 (t, 2H, J = 7); 6.72 (dd, 1H, J = 2, J = 4); 7.01–7.58 (m, 10H); 7.96 (d, 1H, J = 2); 8.86 (s, 1H); 11.03 (br s, 1H). MW 495.51. Anal. Calcd for $C_{27}H_{22}N_7O_2F$: C, 65.45; H, 4.48; N, 19.79. Found: C, 65.09; H, 4.36; N, 19.56.

3.1.1.48. 5-[(4-Chlorophenoxymethyl)carbonyl]amino-8-(3-phenylpropyl)-2-(2-furyl)-pyrazolo[4,3-*e*]1,2,4-triazolo[1,5-*c*] pyrimidine (186). Yield 95%, pale yellow solid; mp 166 °C (EtOAc–light petroleum); IR (KBr): 3225–2985, 1675, 1612, 1578, 1513 cm^{-1}; ^{1}H NMR ($CDCl_3$) δ: 2.24 (t, 2H, J = 7); 2.48–2.59 (m, 2H); 4.38 (t, 2H, J = 7); 5.12 (s, 2H); 6.61 (dd, 1H, J = 2, J = 4); 6.97 (d, 2H, J = 9); 7.05–7.45 (m, 8H); 7.80 (d, 1H, J = 2); 8.47 (s, 1H); 10.32 (br s, 1H). MW 527.96. Anal. Calcd for $C_{26}H_{22}N_7O_3Cl$: C, 63.34; H, 4.33; N, 19.15. Found: C, 63.01; H, 4.30; N, 19.27.

3.1.1.49. 5-[(2,6-Dichlorobenzyl)carbonyl]amino-8-(2-phenylpropyl)-2-(2-furyl)-pyrazolo[4,3-*e*]1,2,4-triazolo[1,5-*c*]pyrimidine (187). Yield 86%, pale yellow solid; mp 210 °C (EtOAc–light petroleum); IR (KBr): 3225–2993, 1679, 1610, 1575, 1508 cm^{-1}; ^{1}H NMR ($CDCl_3$) δ: 2.25 (t, 2H, J = 7); 2.46–2.58 (m, 2H); 4.40 (t, 2H, J = 7); 4.99 (s, 2H); 6.62 (dd, 1H, J = 2, J = 4); 7.08–7.40 (m, 9H); 8.20 (d, 1H, J = 2); 9.22 (s, 1H); 11.53 (br s, 1H). MW 546.41. Anal. Calcd for $C_{27}H_{21}N_7O_2Cl_2$: C, 59.35; H, 3.87; N, 17.94. Found: C, 59.61; H, 3.94; N, 17.78.

4. Biology

4.1. Binding at human A_1, A_{2A}, and A_3 adenosine receptors

All pharmacological methods followed the procedures as described earlier.[49] In brief, membranes for radioligand binding were prepared from CHO cells stably transfected with human adenosine receptor subtypes in a two-step procedure. In a first low-speed step (1000*g*) cell fragments and nuclei were removed. The crude membrane fraction was sedimented from the supernatant at 100,000*g*. The membrane pellet was resuspended in the buffer used for the respective binding experiments, frozen in liquid nitrogen and stored at −80 °C. For the measurement of adenylyl cyclase activity only one high speed centrifugation of the homogenate was used. The resulting crude membrane pellet was resuspended in 50 mM Tris/HCl, pH 7.4 and immediately used for the cyclase assay.

For radioligand binding at A_1 adenosine receptors 1 nM [^{3}H]CCPA was used, whereas 30 and 10 nM [^{3}H]NECA were used for A_{2A} and A_3 receptors, respectively. Non-specific binding of [^{3}H]CCPA was determined in the presence of 1 mM theophylline, in the case of [^{3}H]NECA 100 μM R-PIA was used.[49]

4.2. Functional assay for A_{2B} antagonists

Due to the lack of a suitable A_{2B} radioligand the potency of antagonists was determined in adenylyl cyclase experiments. The procedure was carried out as described previously with minor modifications.[50] Membranes were incubated with about 150,000 cpm of [α-^{32}P]ATP for 20 min in the incubation mixture as described without EGTA and NaCl. For agonists the EC_{50}-values for the stimulation of adenylyl cyclase were calculated with the Hill equation. Hill coefficients in all experiments were near unity. IC_{50} values for concentration-dependent inhibition of NECA-stimulated adenylyl cyclase caused by antagonists was calculated accordingly. Dissociation constants (K_i) for antagonist were then calculated with the Cheng and Prusoff equation.[51]

5. Result and discussion

5.1. General strategy

Support Vector Machine represents a group of supervised learning techniques, firstly applied in pattern recognition, which find now diverse applications in classification and regression problems.[13,14] SVM has been originally developed in fact for classification, then the introduction of a suitable ε-insensitive loss function together with the advantages of the kernel representation, have enabled its application in the regression analysis. In the last years, the use of SVM approach and SVR has helped to solve several classification problems, as for example active and non-active compounds discrimination, and to derive quantitative structure–activity relationships for the prediction of different chemical and biological properties.[15–19,23] SVR seems to be a promising tool, with good generalization performance and increased robustness compared with the traditional neural networks.[52,53]

Furthermore, over the last few years we have stressed the concept that both topological and electrostatic complementarities are considered two key concepts in the molecular recognition processes. We consider this conception extremely crucial in describing the receptor subtypes selectivity. Gasteiger and collaborators investigated the MEP on the molecular surface as a particularly useful method for rationalizing the interactions between molecules and molecular recognition processes.[38,43,44] The introduction of the autocorrelation vector allows then for overcoming the MEP information inconvenience to be reliant on the spatial rotation and translation of the molecule. We have already demonstrated that the *auto*MEP vectors can be used as interesting molecular descriptors in different 3D-QSAR applications.[24–28] In this context, we have also reported that pyrazolo-triazolo-pyrimidine is a versatile scaffold to cover a large spectrum of the adenosine receptor selectivity. In particular, pyrazolo-triazolo-pyrimidines bearing specific substitutions at the N^5 and N^8 positions have been described as highly potent and selective human A_3R antagonists while the position N^7 shifts the selectivity profile to the human A_{2A}R subtype.[11,12] However, even if the N^5–N^7–N^8 substitutability rule seems help to work as a selectivity thumb rule, it is not absolutely trivial to correctly assigned the selectivity profile of a new pyrazolo-triazolo-pyrimidine antagonists.

In this paper, we present an integrated approach based on the presence of two distinct Support Vector Machine tools both using as input matrix the above mentioned *auto*MEP vectors. The first tool is a SVM-driven selectivity *classificator* and the second one a couple of SVR-driven receptor-affinity *predictors*. The workflow of the abovementioned procedure is summarized in Figure 1.

The basic idea beyond our approach is to use the autocorrelated molecular descriptors encoding for the Molecular Electrostatic Potential (*auto*MEP) of each pyrazolo-triazolo-pyrimidine antagonist to optimize the experimental A_{2A}R/A_3R subtypes selectivity profile using a SVM classificator (*auto*MEP/SVM*class*). Once a statistically acceptable *auto*MEP/SVM*class* model has been derived, the two different A_{2A}R and A_3R receptor-affinity predictors can be generated

using even in this case the *auto*MEP descriptors as input values. Following our previously experience in developing valuable tools for the prediction of receptor subtypes selectivity, the use of the *auto*MEP/SVM*class* model ahead of the two receptor-affinity predictors can reduce the number of misattributed compounds that usually derived from the simple ratio between the two predicted $A_{2A}R$ and A_3R receptor-affinity values. In fact, the receptor binding predictions are typically accompanied by a standard errors that compromise the accuracy of their ratio values. In principle, for any external new pyrazolo-triazolo-pyrimidine analog, after calculating its *auto*MEPs, it could be possible to simultaneously access at both $A_{2A}R/A_3R$ subtypes selectivity profile and A_{2A}/A_3R receptor-affinity values.

5.2. SVM classification model (*auto*MEP/SVM*class*)

To construct our SVM-driven selectivity *classificator*, we have selected 104 'selective' pyrazolo-triazolo-pyrimidines derivatives (**1–104**), and we have defined them as our training set. The selectivity profile ($hA_{2A}R$ versus hA_3R) is summarized in Figure 2a.

The definition of 'selectivity' used for our classification approach is based on a simple binary criteria. In particular, the binary criteria acts as simple on–off switch: the selectivity index is set to '+1' if it is referred to a selective $hA_{2A}R$ antagonist, and is '−1' for a selective hA_3R antagonists. Moreover, we have considered as selectivity threshold a difference of at least two orders of magnitude between the corresponding K_i values.

Information encoded by the *auto*MEP vectors has been used as input matrix for our SVM classification protocol. Using a Gaussian radial basis function kernel, several classification models have been generated analyzing all possible combination of the *C* parameter (from 10 to 150 with an interval of 10) and the γ parameter (from 0.001 to 0.015 with an interval of 0.001). The optimized model has been obtained setting the *C* parameter value to 150 and the γ parameter value to 0.01 as shown in Figure 2b. This model has been subjected to an extensive *n*-fold validation procedure and the results are collected in Table 2a. The model sensitivity and specificity, computed from the confusion matrix after leave-one-out cross-validation procedure, are summarized in Table 2b.

The percentages obtained after repeated 10-fold and fivefold validation processes confirm the statistical reliability of this model. Interestingly, it yielded around 90% correct predictions after leave-one-out cross-validation. The statistical robustness is also confirmed by the values of sensitivity and specificity. We consider this percentage amount as an acceptable threshold to validate the robustness of this model to appropriately infer about $hA_{2A}R$ versus hA_3R selectivity spectrum for novel, but structurally related, antagonists. Therefore, we decided to select this model as SVM-driven selectivity *classificator* for the final validation step, described in the validation paragraph.

5.3. SVR regression model (*auto*MEP/SVR)

A different collection of 104 selective pyrazolo-triazolo-pyrimidines analogs (**1–71**, **105–137**) has been selected as training set of known hA_{2A} and hA_3 adenosine receptor antagonists to derive our *auto*MEP/SVR model. In this specific case, the selection of all training set candidates has not necessarily related to their selectivity profiles due to the fact that the principal aim of our predictor is to accurately predict the receptor-binding affinity independently to their spectrum selectivity. Indeed, we have utilized 17 $hA_{2A}R$ selective antagonists, 54 hA_3R selective antagonists and 33 non-selective antagonists, as summarized in Figure 3.

Also in this step, information encoded by the *auto*MEP vectors of all training set antagonists has been used as input matrix for our SVR prediction protocol. For the generation of both regression

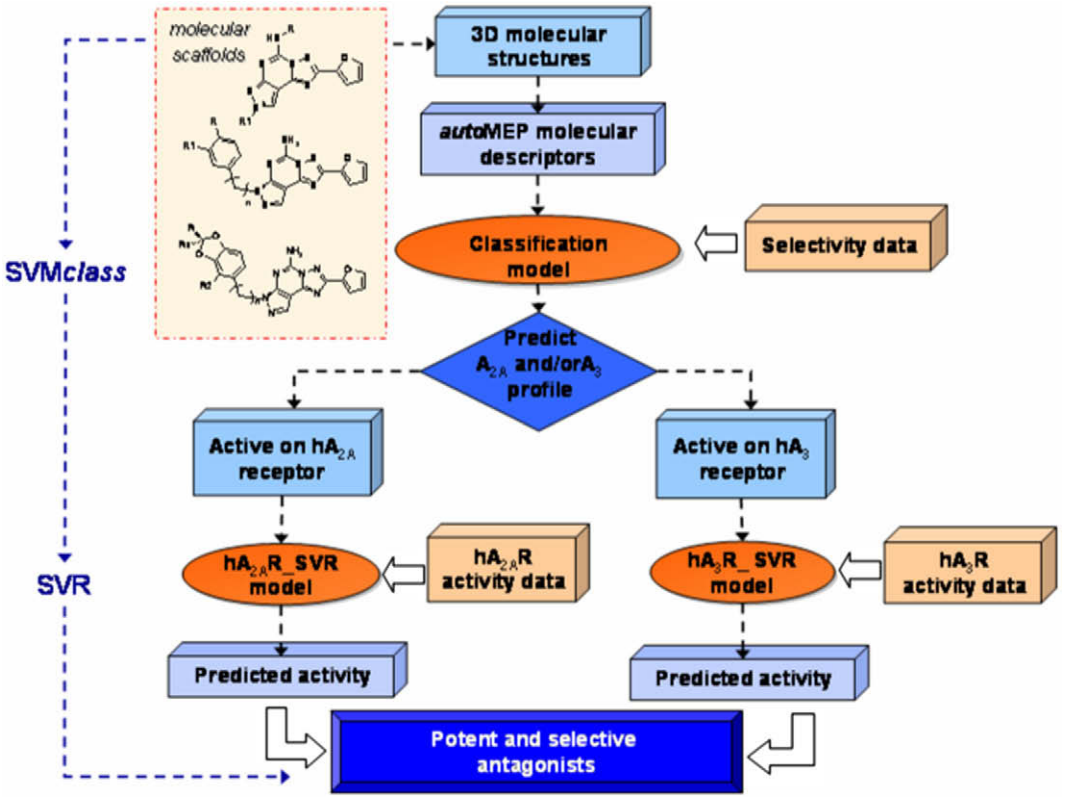

Figure 1. Flowchart of the in series autoMEP/SVM*class* and autoMEP/SVR approach for the selection of new selective and potent human A_{2A} and A_3 receptor antagonists.

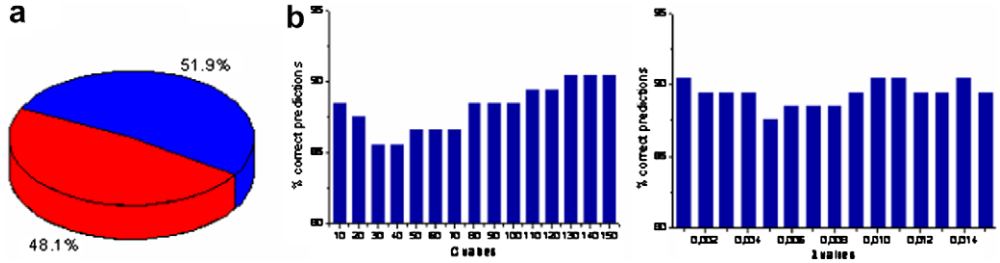

Figure 2. SVM*class* finally selected model (104 molecules). (a) Data distribution indicating the percentage % of $hA_{2A}R$ antagonists (■—red) and the percentage% of hA_3R antagonists (■—blue) in the training set (50 hA_{2AR} and 54 hA_3R antagonists); (b) parameter selection in SVM*class* model: percentage % of correct prediction in leave-one-out validation procedure selecting different values of C ($\gamma = 0.01$) and selecting different values of γ ($C = 150$).

Table 2a
*Auto*MEP/SVM*class* model: the statistical parameters after the cross-validation procedure on the selected classificator are collected

Partition	CV	No. of runs	% Correct predictions			
			Mean	Stdev	Min	Max
Training set		1	99.0	—	99.0	99.0
Training set	LOO	1	93.3	—	93.3	93.3
	10-fold	10	91.4	2.5	86.5	95.2
	Fivefold	10	91.7	2.1	88.5	94.2
Test set		1	78.4	—	78.4	78.4

Table 2b
*Auto*MEP/SVM*class* model: the statistical parameters after the LOO cross-validation procedure are reported

	Correct predictions (%)	Sensitivity (%)	Specificity (%)
LOO-cv	93.3	92.0	94.4

models, also in this case we have utilized a Gaussian radial basis function kernel. In the case of A_{2A} model several prediction models have been generated analyzing all possible combination of the C parameter (from 50 to 200 with an interval of 10), the ε parameter (from 0.0005 to 0.001 with an interval of 0.0001 and from 0.001 to 0.005 with an interval of 0.001) and the γ parameter (from 0.0005 to 0.001 with an interval of 0.0001 and from 0.001 to 0.005 with an interval of 0.001). Slightly different combinations of these parameters have been used for the generation of the optimized hA_3R SVR model (the C parameter has been changed from 50 to 200 with an interval of 10, the ε parameter from 0.1 to 0.9 with an interval of 0.1 and the γ parameter from 0.005 to 0.05 with an interval of 0.01).

An acceptable $hA_{2A}R$ SVR model ($C = 200$, $\varepsilon = 0.0005$, $\gamma = 0.0006$, as showed in Fig. 4) has been obtained as indicated by the leave-one-out cross-validated correlation coefficient (r_{cv}) of 0.78 and a root mean square of residuals (RMSR) of 0.050. *auto*MEP/SVR statistical parameters are summarized in Figure 4.

On the other hand, the best hA_3R SVR predictor ($C = 150$, $\varepsilon = 0.3$, $\gamma = 0.005$, as reported in Fig. 5) has been obtained as described by the leave-one-out cross-validated correlation coefficient (r_{cv}) of 0.85 and a root mean square of residuals (RMSR) of 0.046. *auto*MEP/SVR statistical parameters are summarized in Figure 5.

The results of SVR analysis are noteworthy considering that the same training set has been used to generated two different robust models. Both predictors in the validation step are described in the following paragraph. An alternative non-linear modeling strategy, Response Surface Analysis (RSA), has been performed using the same training and test sets. Even if the models robustness is similar, the SVR predictions on the test set for both $hA_{2A}R$ and hA_3R models are notably better than the results of the respective RSA selected predictors. See Supplementary data for details.

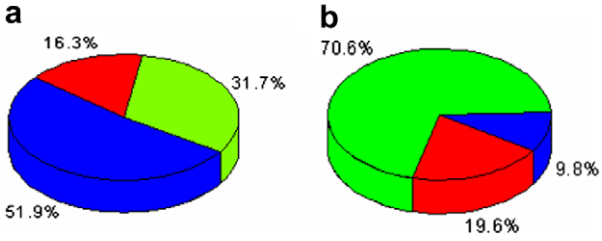

Figure 3. Data distribution representation indicating the percentage % of selective $hA_{2A}R$ antagonists (■—red), the percentage % of selective hA_3R antagonists (■—blue) and the percentage % of non-selective compounds (■—green): (a) in the training set of SVR $hA_{2A}R$ and SVR hA_{3R} models (17 $hA_{2A}R$ and 54 hA_3R antagonists, 33 non-selective antagonists); (b) in the test set (10 $hA_{2A}R$ and 5 hA_3R antagonists, 36 non-selective antagonists, including 17 more active on $hA_{2A}R$ antagonists and 19 more active on hA_3R antagonists).

5.4. Validation of the tandem *auto*MEP/SVM*class* and *auto*MEP/SVR models

As anticipated, the principal aim of the present work has been to evaluate the robustness of the tandem *auto*MEP/SVM*class* and *auto*MEP/SVR in the prediction of both $A_{2A}R/A_3R$ subtypes selectivity and receptor binding affinity profiles of new pyrazolo-triazolo-pyrimidines derivatives.

To achieve to this objective, 51 novel pyrazolo-triazolo-pyrimidines analogs (**138**–**188**) have been synthetized and pharmacologically characterized. The experimental $A_{2A}R$ and A_3R binding affinities are collected in Table 3. The human A_1R binding affinity and the IC_{50} referring to the inhibition of NECA-stimulated adenylyl cyclase activity in CHO cells expressing human A_{2B} receptors are reported in the Table 1. Moreover, the experimental spectrum of selectivity is summarized in Figure 3. We also performed a Principal Component Analysis (PCA) to explore the similarity between the compounds used as training set in the *auto*MEP/SVM*class* model and the novel selective $hA_{2A}R$ (molecules **142**, **153**, **155**, **156**, **159**, **170**, **172**, **174**–**176** in Table 3) and hA_3R antagonists (molecules **139**, **141**, **145**, **152**, **181** in Table 3) in the test set.[54] Chemical information encoded in both $hA_{2A}R$ and hA_3R antagonists was compared by considering the *auto*MEP vectors as variables in the PCA. According to this analysis, the closer two molecules are in the score plot, the higher is their similarity with respect to the components concerned. Figure 6 shows the overlap between the training set and test set chemical spaces.[55]

Following the workflow reported in Figure 1, the *auto*MEP vectors of these new 51 antagonists have been used as input matrix for the previously generated *auto*MEP/SVM*class* classificator. As previously shown in Table 2a, our classification model was able to correctly assign the 78% of the compounds in the collected test

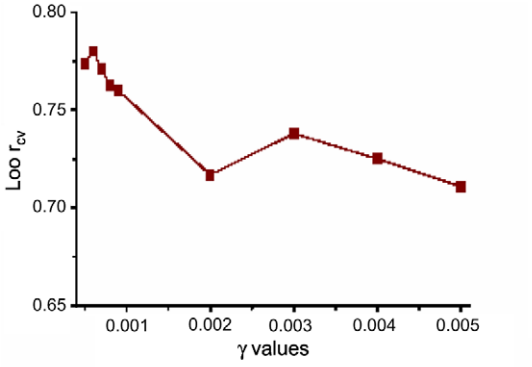

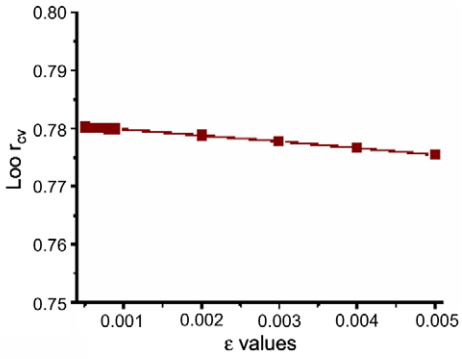

	SVR $hA_{2A}R$ model
Number of molecules	104
r	0.83
r_{cv} [a]	0.78
Slope	0.62
Offset	-0.71
RMSR[b]	0.050

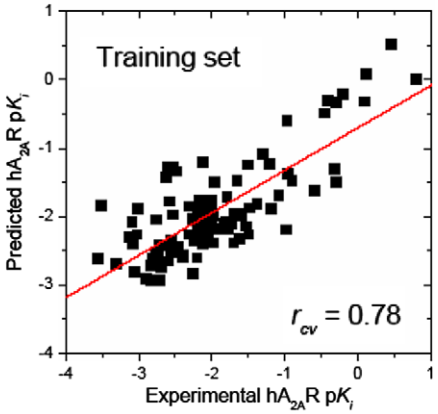

Figure 4. *Auto*MEP/SVR $hA_{2A}R$ model results. (a) Cross-validated r after leave-one-out procedure: r_{cv} = [SXY/(SXX)1/2(SYY)1/2], SXY = $\sum(X - X_{mean})(Y - Y_{mean})$, SXX = $\sum(X - X_{mean})^2$ and SYY = $\sum(Y - Y_{mean})^2$ with $X = Y_{experimental}$ and $Y = Y_{predicted}$; (b) RMSR: root mean square of residuals.

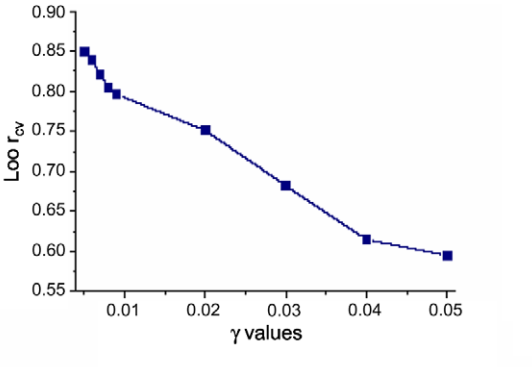

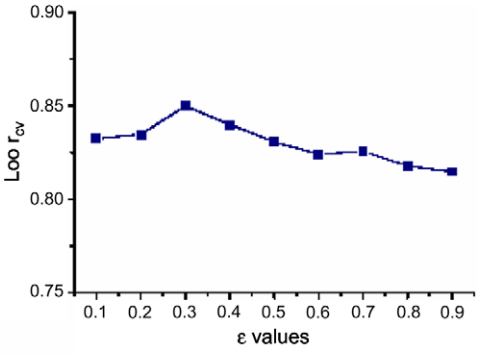

	SVR hA_3R model
Number of molecules	104
r	0.95
r_{cv} [a]	0.85
Slope	0.75
Offset	-0.11
RMSR[b]	0.046

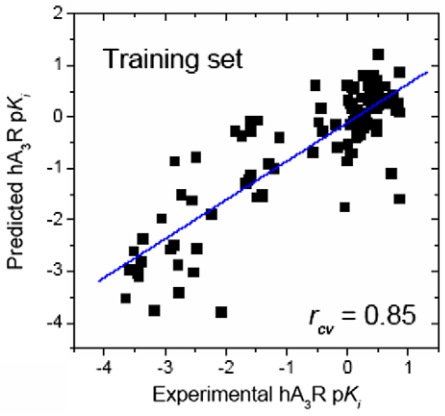

Figure 5. *Auto*MEP/SVR hA_3R model results. (a) Cross-validated r after leave-one-out procedure: r_{cv} = [SXY/(SXX)1/2(SYY)1/2], SXY = $\sum(X - X_{mean})(Y - Y_{mean})$, SXX = $\sum(X - X_{mean})^2$ and SYY = $\sum(Y - Y_{mean})^2$ with $X = Y_{experimental}$ and $Y = Y_{predicted}$; (b) RMSR: root mean square of residuals.

Table 3
Predicted and experimental $hA_{2A}R$ and hA_3R both pK_i *and* K_i for the test set

Pred pK_i (nM) $hA_{2A}R$	Exp pK_i (nM) $hA_{2A}R$	ΔpK_i^*	Pred K_i (nM) $hA_{2A}R$	Exp K_i (nM) $hA_{2A}R$	#	Exp K_i (nM) hA_3R	Pred K_i (nM) hA_3R	ΔpK_i^*	Exp pK_i (nM) hA_3R	Pred pK_i (nM) hA_3R
−2.25	−2.48	0.23	177.83	305	**138**	343	107.15	0.51	−2.54	−2.03
−1.79	−2.33	0.54	61.66	216	**139**	0.25	0.47	−0.27	0.60	0.33
−2.04	−2.29	0.25	109.65	193	**140**	11.2	35.48	−0.50	−1.05	−1.55
−2.07	−2.20	0.13	117.49	159	**141**	5.86	2.88	0.31	−0.77	−0.46
−1.05	−0.96	−0.09	11.22	9.18	**142**	268	144.54	0.27	−2.43	−2.16
−1.47	−1.73	0.26	29.51	53.1	**143**	6.49	1.70	0.58	−0.81	−0.23
−1.18	−1.67	0.49	15.14	46.9	**144**	125	70.79	0.25	−2.10	−1.85
−1.85	−2.06	0.21	70.79	114	**145**	1.2	0.56	0.33	−0.08	0.25
−1.21	−1.60	0.39	16.22	39.6	**146**	189	51.29	0.57	−2.28	−1.71
−1.59	−1.48	−0.11	38.90	30.5	**147**	1.94	2.24	−0.06	−0.29	−0.35
−1.87	−1.67	−0.20	74.13	46.5	**148**	0.93	0.60	0.19	0.03	0.22
−1.15	−1.72	0.57	14.13	52.5	**149**	65.4	44.67	0.17	−1.82	−1.65
−1.67	−2.19	0.52	46.77	156	**150**	12.7	6.92	0.26	−1.10	−0.84
−1.41	−1.85	0.44	25.70	70.9	**151**	14.2	72.44	−0.71	−1.15	−1.86
−1.78	−1.80	0.02	60.26	62.5	**152**	0.95	3.39	−0.55	0.02	−0.53
−1.32	−1.20	−0.12	20.89	15.7	**153**	409	85.11	0.68	−2.61	−1.93
−1.12	−1.62	0.50	13.18	42.1	**154**	180	46.77	0.59	−2.26	−1.67
−1.41	−0.94	−0.47	25.70	8.8	**155**	330	269.15	0.09	−2.52	−2.43
−1.58	−1.11	−0.47	38.02	12.9	**156**	726	707.95	0.01	−2.86	−2.85
−1.65	−1.87	0.22	44.67	74.6	**157**	3.05	11.48	−0.58	−0.48	−1.06
−1.52	−1.26	−0.26	33.11	18.4	**158**	36.3	23.99	0.18	−1.56	−1.38
−1.73	−1.36	−0.37	53.70	23	**159**	765	489.78	0.19	−2.88	−2.69
−1.52	−1.20	−0.32	33.11	15.9	**160**	196	186.21	0.02	−2.29	−2.27
−1.64	−1.75	0.11	43.65	56	**161**	5.26	1.12	0.67	−0.72	−0.05
−1.71	−1.50	−0.21	51.29	31.3	**162**	1.25	3.55	−0.45	−0.10	−0.55
−1.63	−1.89	0.26	42.66	77.5	**163**	14.5	3.55	0.61	−1.16	−0.55
−1.79	−1.91	0.12	61.66	80.5	**164**	3.47	2.51	0.14	−0.54	−0.40
−1.69	−1.59	−0.10	48.98	38.7	**165**	17.3	67.61	−0.59	−1.24	−1.83
−0.99	−0.90	−0.09	9.77	7.99	**166**	95.9	57.54	0.22	−1.98	−1.76
−1.48	−1.07	−0.41	30.20	11.7	**167**	100	61.66	0.21	−2.00	−1.79
−1.76	−1.88	0.12	57.54	75.9	**168**	1.22	18.20	−1.17	−0.09	−1.26
−1.41	−0.62	−0.79	25.70	4.15	**169**	99.8	173.78	−0.24	−2.00	−2.24
−0.76	−0.50	−0.26	5.75	3.13	**170**	189	22.39	0.93	−2.28	−1.35
−1.06	−1.59	0.53	11.48	39.3	**171**	223	52.48	0.63	−2.35	−1.72
−0.23	−0.27	0.04	1.70	1.86	**172**	273	97.72	0.45	−2.44	−1.99
0.11	−0.44	0.55	0.78	2.75	**173**	56.5	125.89	−0.35	−1.75	−2.10
−1.23	−0.76	−0.47	16.98	5.75	**174**	273	169.82	0.21	−2.44	−2.23
−0.86	−0.73	−0.13	7.24	5.43	**175**	266	89.13	0.47	−2.42	−1.95
−0.14	−0.57	0.43	1.38	3.69	**176**	116	173.78	−0.18	−2.06	−2.24
−1.93	−1.73	−0.20	85.11	54.1	**177**	0.97	14.45	−1.17	0.01	−1.16
−0.85	−1.27	0.42	7.08	18.7	**178**	207	112.20	0.27	−2.32	−2.05
−1.32	−1.66	0.34	20.89	45.2	**179**	44.4	8.51	0.72	−1.65	−0.93
−1.96	−2.32	0.36	91.20	211	**180**	58.5	223.87	−0.58	−1.77	−2.35
−2.34	−2.51	0.17	218.78	326	**181**	12.6	2.82	0.65	−1.10	−0.45
−1.82	−1.87	0.05	66.07	73.6	**182**	717	524.81	0.14	−2.86	−2.72
−1.33	−1.64	0.31	21.38	43.9	**183**	5.49	14.79	−0.43	−0.74	−1.17
−2.07	−2.26	0.19	117.49	182	**184**	110	245.47	−0.35	−2.04	−2.39
−1.26	−1.95	0.69	18.20	89.9	**185**	30.5	213.80	−0.85	−1.48	−2.33
−1.29	−1.43	0.14	19.50	27.2	**186**	400	602.56	−0.18	−2.60	−2.78
−2.48	−2.27	−0.21	302.00	186	**187**	601	1258.93	−0.32	−2.78	−3.10
−2.18	−2.41	0.23	151.36	256	**188**	410	48.98	0.92	−2.61	−1.69

Differences between predicted and experimental pK_i values for both SVR models ($hA_{2A}R$ and hA_3R) are reported.
* Predicted pK_i—experimental pK_i.
In the middle column $hA_{2A}R$ selective antagonists (■—red) and hA_3R selective antagonists (■—blue) are highlighted.

set to their class. In more detail, a sensitivity of 92.0% and a specificity of 65.4% were achieved by predicting the test set. Surprisingly, almost all the selective compounds of our test set are correctly classified and only 11 of them (22%) have been erroneously recognized (Tables 4a, and b).

Analyzing in more detail these 11 derivatives, we can consider these as 'tricky' cases considering both the entity of the corresponding experimental errors, and the similarity between their $hA_{2A}R$ and hA_3R K_i values. Even if preliminary, we consider the performance of this selectivity classificator very encouraging.

After passing the selectivity filtering process, each of the $hA_{2A}R$ and hA_3R antagonist has been analyzed by the corresponding SVR binding affinity predictor. The comparison of all the experimental with the predicted pK_i values by the abovementioned $hA_{2A}R$ and hA_3R SVR models on the test set again support the quality of the predictors, as underlined by the good values of the correlation coefficient ($q = 0.82$ and $q = 0.85$, respectively) (Figs. 6a and 7aa). In Figures 6b and 7b only the hA_{2A} classified antagonists predicted by the $hA_{2A}R$ SVR model and only the hA_3A classified antagonists predicted by the hA_3R SVR model respectively have been reported. The prediction accuracies, as demonstrated by the differences between the experimental and the predicted pK_i, are statistically satisfying for both $hA_{2A}R$ and hA_3R SVR models, with few exceptions in particular regarding the hA_3R binding affinity prediction such as **168**, **170**, **185** and **188** (see Table 3, Figs. 7b and 8b).

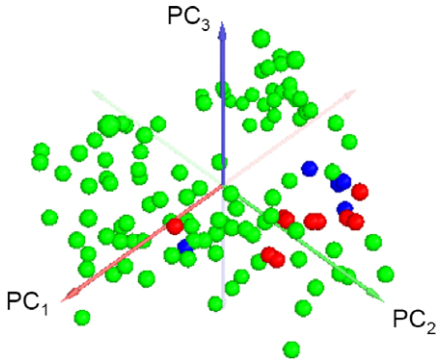

Figure 6. Graphical representation of the scores resulting from the Principal Component Analysis (PCA) by using 12 *auto*MEP vectors for each molecule as variables. The compounds included in the training set of the *auto*MEP/SVM*class* classificator (●—green), selective $hA_{2A}R$ antagonists (●—red) and hA_3R antagonists (●—blue) in the test set are plotted. The projections for each compound on the first three principal components have been considered.

Table 4b
*auto*MEP/SVM*class* model: both predicted and experimental hA_3R classification results are reported for the classified hA_3R compounds in the test set

Mol classified hA_3R	Pred higher affinity on hA_3R	Exp higher affinity on hA_3R
139	Yes	Yes
141	Yes	Yes
143	Yes	Yes
145	Yes	Yes
147	Yes	Yes
148	Yes	Yes
150	Yes	Yes
152	Yes	Yes
157	Yes	Yes
159	Yes	No ($hA_{2A}R$, selective)
160	Yes	No ($hA_{2A}R$, non-selective)
161	Yes	Yes
162	Yes	Yes
163	Yes	Yes
164	Yes	Yes
165	Yes	Yes
168	Yes	Yes
177	Yes	Yes
179	Yes	Yes

In the first column the correctly classified hA_3R antagonists—true positive—(■—green) are highlighted.

5.5. Structure–activity relationship analysis

All newly synthesized pyrazolo-triazolo-pyrimidines (**138–188**) were tested against all four human adenosine receptor subtypes.

The data summarized in Table 1 show that all the tested compounds **138–188** display a broad affinity spectrum against the four adenosine receptor subtypes with different levels of receptor subtypes selectivity.

It is clearly evident, as previously observed for the pyrazolo-triazolo-pyrimidines as human A_3 adenosine receptor antagonists, that the presence of a methyl group at the N^8 position seems to confer a better profile at the hA_3 adenosine receptor with an affinity in the low nanomolar range independently from the substitution at the N^5 position (e.g., compounds **147, 150, 152, 161–164, 168**) with good levels of selectivity vs the other receptor subtypes. The effect of the methyl substitution at the N^8 position is well described by both *auto*MEP/SVM*class* and *auto*MEP/SVR models, as highlighted in Tables 3, 4a and b.

Interestingly, a quite different binding profile was observed when at the N^8 position bulkier groups than a methyl substituent were

Table 4a
*Auto*MEP/SVM*class* model: both predicted and experimental $hA_{2A}R$ classification results are reported for the classified $hA_{2A}R$ compounds in the test set

Mol classified $hA_{2A}R$	Pred higher affinity on $hA_{2A}R$	Exp higher affinity on $hA_{2A}R$	Mol classified $hA_{2A}R$	Pred higher affinity on $hA_{2A}R$	Exp higher affinity on $hA_{2A}R$
138	Yes	Yes	171	Yes	Yes
140	Yes	No (hA_3R, non-selective)	172	Yes	Yes
142	Yes	Yes	173	Yes	Yes
144	Yes	Yes	174	Yes	Yes
146	Yes	Yes	175	Yes	Yes
149	Yes	Yes	176	Yes	Yes
151	Yes	No (hA_3R, non-selective)	178	Yes	Yes
153	Yes	Yes	**180**	Yes	No (hA_3R, non-selective)
154	Yes	Yes	**181**	Yes	No (hA_3R, selective)
155	Yes	Yes	182	Yes	Yes
156	Yes	Yes	**183**	Yes	No (hA_3R, non-selective)
158	Yes	Yes	**184**	Yes	No (hA_3R, non-selective)
166	Yes	Yes	**185**	Yes	No (hA_3R, non-selective)
167	Yes	Yes	186	Yes	Yes
169	Yes	Yes	**187**	Yes	No (hA_3R, non-selective)
170	Yes	Yes	**188**	Yes	No (hA_3R, non-selective)

In the first column the correctly classified $hA_{2A}R$ antagonists—true positive—(■—green) are highlighted.

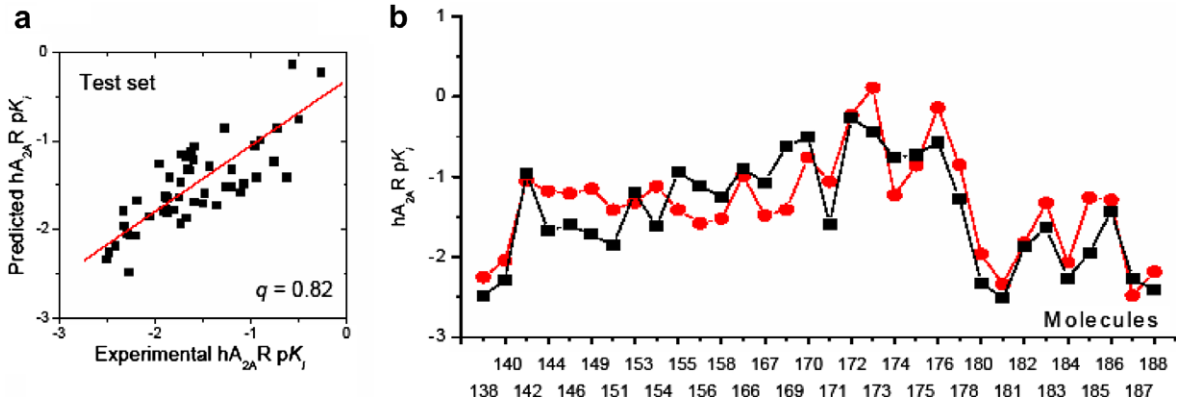

Figure 7. (a) Experimental pK_i activity data plotted versus Predicted pK_i values by the *auto*MEP/SVR hA_{2A}R model for the test set; (b) experimental pK_i activity data (■—black) of the classified selective hA_{2A}R antagonists included in the test set compared to pK_i values predicted by *auto*MEP/SVR hA_{2A}R model (●—red).

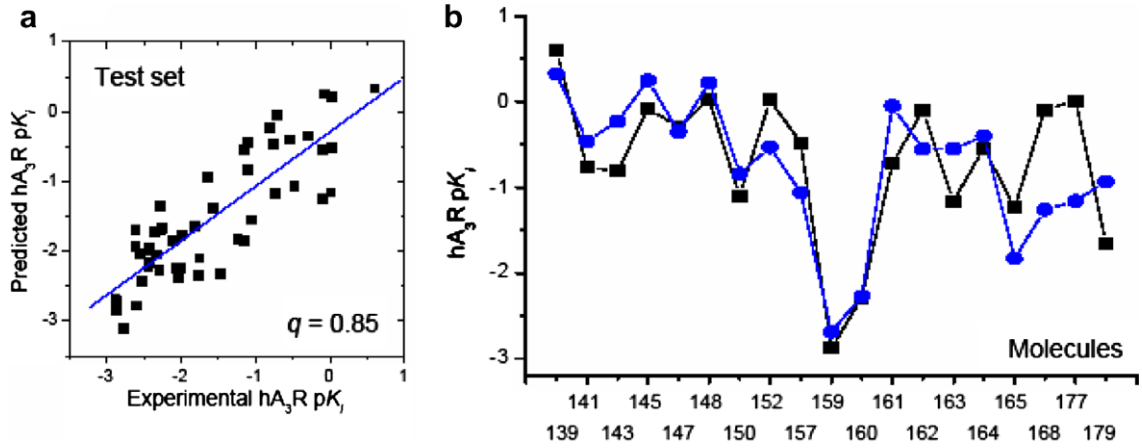

Figure 8. (a) Experimental pK_i activity data plotted versus Predicted pK_i values by the *auto*MEP/SVR hA_3R model for the test set; (b) experimental pK_i activity data (■—black) of the classified selective hA_{A3}R antagonists included in the test set compared to pK_i values predicted by *auto*MEP/SVR hA_3R model (●—blue).

introduced. In fact, when ethyl, propyl or *n*-butyl groups are linked at the N^8 pyrazole nitrogen in combination with several arylacetyl moieties at the N^5 position, a major change in binding affinities were detected and consequently a shift of selectivity spectrum was also observed. In particular, the presence of a 2-thienyl or 3-thienyl groups at the N^5 position significantly increase the affinity at the hA_{2A}R while a significant reduction of affinity at the hA_3R was observed, with a resulting increase of selectivity vs this receptor subtype (e.g., compound **170**: K_ihA_1 = 25.5 nM, K_ihA_{2A} = 3.13 nM, IC_{50}hA_{2B} = 906 nM, K_ihA_3 = 189 nM). Also in this specific case, our predictions seem to be very closed to the experimental data.

Another interesting convergent scenario between predicted and experimental results regards the influence on the affinity of the naphthylacetyl moiety at the N^5 position. In fact comparing the α and β isomers it is clearly evident that while the α-isomer retains good potency and selectivity for the hA_3 adenosine receptor (e.g., compound **157**: K_ihA_1 = 596 nM, K_ihA_{2A} = 74.6 nM, IC_{50}hA_{2B} = 50,000 nM, K_ihA_3 = 3.05 nM), the β-isomer resulted to be more potent for the hA_{2A} subtype (e.g., compound **158**: K_ihA_1 = 185 nM, K_ihA_{2A} = 18.4 nM, IC_{50}hA_{2B} = 10,370 nM, K_ihA_3 = 36.3 nM).

Among this series, significant differences in terms of affinity could be observed when at the N^8 position a branched chain, such as isopentyl, is present. In fact, all the derivatives bearing this substitution at the N^8 position, independently from the substitutions at the N^5 position showed the best affinity versus the hA_{2A} adenosine receptors (e.g., compound **175**: K_ihA_1 = 48.2 nM, K_ihA_{2A} = 5.43 nM, IC_{50}hA_{2B} = 5480 nM, K_ihA_3 = 266 nM) with the exception of compound **141** (K_ihA_1 = 441 nM, K_ihA_{2A} = 159 nM, IC_{50}hA_{2B} = >10,000 nM, K_ihA_3 = 5.86 nM), which still retains good affinity for the hA_3 adenosine receptor. A quite similar behavior could be detected when bulky substituents (phenylethyl or phenylpropyl) are linked at the N^8 position: In fact in general, with the exception of some substituents at the N^5 position (e.g., diphenylacetyl: compounds **143** and **181**), all the derivatives showed a binding profile favorable to the A_{2A} adenosine receptors but the levels of selectivity are very low.

In contrast with our previous studies, it seems that a combination of bulky substituents at the N^5 and N^8 positions (e.g., compounds **138** and **154**) resulted to be detrimental in term of affinity at the four adenosine receptors subtypes and in particular, as theoretically demonstrated, at the A_{2B} adenosine receptors. Also in this case, a good correspondence between predicted and experimental results has been found.

6. Conclusions and perspectives

In the present work, we have presented a combination of Support Vector Machine tools able to predict both A_{2A}R versus A_3R subtypes selectivity profile and the corresponding receptor binding affinities of a large dataset of known pyrazolo-triazolo-pyrimidine analogs. The preliminary results based on a new set of 51 pyrazolo-triazolo-pyrimidines are very encouraging. To further validate our integrated SVM approach, we are extending the applicability of this method to other class of A_{2A}R and A_3R antagonists and, at the same

time, we are exploring the possibility to achieve, using a multi-classificator, to the full adenosine selectivity spectrum (from the human A_1R to the A_3 subtype).

Acknowledgments

The molecular modeling work coordinated by S.M. was carried out with financial support from the University of Padova, Italy, and the Italian Ministry for University and Research (MIUR), Rome, Italy. We thank the Molecular Network GmbH (Erlangen, Germany) for the assistance in using the Adriana modeling suite. S.M. is also very grateful to the Chemical Computing Group for the scientific and technical partnership.

Supplementary data

Supplementary data (Training sets (Tables 1 and 2) and test set (Table 3), together with Table 4 of elemental analyses of synthesized compounds) associated with this article can be found, in the online version, at doi:10.1016/j.bmc.2009.05.038.

References and notes

1. Moro, S.; Bacilieri, M.; Deflorian, F.; Spalluto, G. *New J. Chem.* **2006**, *30*, 301.
2. Moro, S.; Deflorian, F.; Bacilieri, M.; Spalluto, G. *Curr. Pharm. Des.* **2006**, *12*, 2175.
3. Fredholm, B. B.; Arslan, G.; Halldner, L.; Kull, B.; Schulte, G.; Wasserman, W. *Naunyn-Schmiedeberg's Arch. Pharmacol.* **2000**, *362*, 364.
4. Jacobson, K. A.; Gao, Z. G. *Nat. Rev. Drug Discovery* **2006**, *5*, 247.
5. Muller, C. E. *Curr. Top. Med. Chem.* **2003**, *3*, 445.
6. Jacobson, K. A. In *Annual Reports in Medicinal Chemistry*; Elsevier: San Diego, CA, 2003.
7. Johnston, T. H.; Brotchie, J. M. *Curr. Opin. Invest. Drugs* **2006**, *7*, 25.
8. Ferre, S.; von Euler, G.; Johansson, B.; Fredholm, B. B.; Fuxe, K. *Proc. Natl. Acad. Sci. U.S.A.* **1991**, *88*, 7238.
9. Ribeiro, J. A.; Sebastiao, A. M.; de Mendonca, A. *Prog. Neurobiol.* **2002**, *68*, 377.
10. Xu, K.; Bastia, E.; Schwarzschild, M. *Pharmacol. Ther.* **2005**, *105*, 267.
11. Baraldi, P. G.; Cacciari, B.; Moro, S.; Spalluto, G.; Pastorin, G.; Da Ros, T.; Klotz, K. N.; Varani, K.; Gessi, S.; Borea, P. A. *J. Med. Chem.* **2002**, *45*, 770.
12. Baraldi, P. G.; Tabrizi, M. A.; Bovero, A.; Avitabile, B.; Preti, D.; Fruttarolo, F.; Romagnoli, R.; Varani, K.; Borea, P. A. *Eur. J. Med. Chem.* **2003**, *38*, 367.
13. Burges, C. J. C. *Data Min. Knowl. Discovery* **1998**, *2*, 121.
14. Cristianini, N.; Shawe-Taylor, J. *An Introduction to Support Vector Machines*; Cambridge University Press, 2000.
15. Czerminski, R.; Yasri, A.; Hartsough, D. *Quant. Struct. Act. Relat.* **2001**, *20*, 227.
16. Warmuth, M. K.; Liao, J.; Ratsch, G.; Mathieson, M.; Putta, S.; Lemmen, C. *J. Chem. Inf. Comput. Sci.* **2003**, *43*, 667.
17. Jorissen, R. N.; Gilson, M. K. *J. Chem. Inf. Model.* **2005**, *45*, 549.
18. Bruce, C. L.; Melville, J. L.; Pickett, S. D.; Hirst, J. D. *J. Chem. Inf. Model.* **2007**, *47*, 219.
19. Liu, H. X.; Zhang, R. S.; Yao, X. J.; Liu, M. C.; Hu, Z. D.; Fan, B. T. *J. Chem. Inf. Comput. Sci.* **2003**, *43*, 1288.
20. Liu, H. X.; Zhang, R. S.; Yao, X. J.; Liu, M. C.; Hu, Z. D.; Fan, B. T. *J. Chem. Inf. Comput. Sci.* **2004**, *44*, 161.
21. Norinder, U. *Neurocomputing* **2003**, *55*, 337.
22. Xue, C. X.; Zhang, R. S.; Liu, H. X.; Yao, X. J.; Liu, M. C.; Hu, Z. D.; Fao, B. T. *J. Chem. Inf. Comput. Sci.* **2004**, *44*, 1693.
23. Oloff, S.; Mailman, R. B.; Tropsha, A. *J. Med. Chem.* **2005**, *48*, 7322.
24. Moro, S.; Bacilieri, M.; Ferrari, C.; Spalluto, G. *Curr. Drug Discovery Technol.* **2005**, *2*, 13.
25. Moro, S.; Bacilieri, M.; Cacciari, B.; Spalluto, G. *J. Med. Chem.* **2005**, *48*, 5698.
26. Moro, S.; Bacilieri, M.; Cacciari, B.; Bolcato, C.; Cusan, C.; Pastorin, G.; Klotz, K. N.; Spalluto, G. *Bioorg. Med. Chem.* **2006**, *14*, 4923.
27. Bacilieri, M.; Kaseda, C.; Spalluto, G.; Moro, S. *Lett. Drug Des. Discovery* **2007**, *4*, 122.
28. Michielan, L.; Bacilieri, M.; Schiesaro, A.; Bolcato, C.; Pastorin, G.; Spalluto, G.; Cacciari, B.; Klotz, K. N.; Kaseda, C.; Moro, S. *J. Comput. Inf. Model.* **2008**, *48*, 350.
29. OPENMOSIX, Version 2.4.26; Moshe Bar, Tel Aviv University, Israel, 2004.
30. ADRIANACODE; Version 2.0; Molecular Networks GmbH: Erlangen, Germany, 2005.
31. Joachims, T. SVM^{light}; Version 6.01; Support Vector Machine. http://svmlight.joachims.org, 2004.
32. Baraldi, P. G.; Cacciari, B.; Romagnoli, R.; Spalluto, G.; Moro, S.; Klotz, K. N.; Leung, E.; Varani, K.; Gessi, S.; Merighi, S.; Borea, P. A. *J. Med. Chem.* **2000**, *43*, 4768.
33. Baraldi, P. G.; Cacciari, B.; Romagnoli, R.; Spalluto, G.; Varani, K.; Gessi, S.; Merighi, S.; Borea, P. A. *Drug Dev. Res.* **2001**, *52*, 406.
34. Baraldi, P. G.; Cacciari, B.; Romagnoli, R.; Spalluto, G.; Monopoli, A.; Ongini, E.; Varani, K.; Borea, P. A. *J. Med. Chem.* **2002**, *45*, 115.
35. Baraldi, P. G.; Cacciari, B.; Spalluto, G.; Bergonzoni, M.; Dionisotti, S.; Ongini, E.; Varani, K.; Borea, P. A. *J. Med. Chem.* **1998**, *41*, 2126.
36. Baraldi, P. G.; Fruttarolo, F.; Tabrizi, M. A.; Preti, D.; Romagnoli, R.; El-Kashef, H.; Moorman, A.; Varani, K.; Gessi, S.; Merighi, S.; Borea, P. A. *J. Med. Chem.* **2003**, *46*, 1229.
37. Baraldi, P. G.; Cacciari, B.; Romagnoli, R.; Klotz, K. N.; Spalluto, G.; Varani, K.; Gessi, S.; Merighi, S.; Borea, P. A. *Drug Dev. Res.* **2001**, *53*, 225.
38. Gasteiger, J.; Li, X.; Rudolph, C.; Sadowski, J.; Zupan, J. *J. Am. Chem. Soc.* **1994**, *116*, 4608.
39. Gasteiger, J.; Marsili, M. *Tetrahedron* **1980**, *36*, 3219.
40. Gasteiger, J.; Saller, H. *Angew. Chem., Int. Ed. Engl.* **1985**, *24*, 687.
41. Moreau, G.; Broto, P. *Nouv. J. Chim.* **1980**, *4*, 757.
42. Moreau, G.; Broto, P. *Nouv. J. Chim.* **1980**, *4*, 359.
43. Wagener, M.; Sadowski, J.; Gasteiger, J. *J. Am. Chem. Soc.* **1995**, *117*, 7769.
44. Bauknecht, H.; Zell, A.; Bayer, H.; Levi, P.; Wagener, M.; Sadowski, J.; Gasteiger, J. *J. Chem. Inf. Comput. Sci.* **1996**, *36*, 1205.
45. Vapnik, V. *The Nature of Statistical Learning Theory*; Springer: New York, 1995.
46. Vapnik, V. *Statistical Learning Theory*; Wiley: New York, 1998.
47. Smola, A. J.; Scholkopft, B. *Learning with Kernels. Support Vector Machines, Regularization, Optimization, and Beyond*; MIT Press, 2002.
48. Smola, A. J.; Scholkopft, B. *A Tutorial on Support Vector Regression*; NeuroCOL Technical Report Series, NCR2-TR-1998-030, 1998.
49. Li, A. H.; Moro, S.; Forsyth, N.; Melman, N.; Ji, X. D.; Jacobson, K. A. *J. Med. Chem.* **1999**, *42*, 706.
50. Klotz, K. N.; Hessling, J.; Hegler, J.; Owman, C.; Kull, B.; Fredholm, B. B.; Lohse, M. J. *Naunyn-Schmiedeberg's Arch. Pharmacol.* **1998**, *357*, 1.
51. Cheng, Y. C.; Prusoff, H. R. *Biochem. Pharmacol.* **1973**, *22*, 3099.
52. Demiriz, A.; Bennett, K. P.; Breneman, C. M.; Embrechts, M. J. *Support Vector Regression in Chemoinformatics* In *Computing Science and Statistics: Proceeding of Interface*; 2001.
53. Ivanciuc, O. *Rev. Comput. Chem.* **2007**, *23*, 291.
54. THE UNSCRUMBLER, Version 9.8; CAMO Process AS: Oslo, Norway, 2008.
55. MOLEGRO DATA MODELLER, Version 1.0.0; Molegro ApS: Aarhus C, Denmark, 2007.